Int J Adv Manuf Technol (2013) 66:917–936
DOI 10.1007/s00170-012-4377-8

ORIGINAL ARTICLE

Two-dimensional pheromone propagation controller applied to run-to-run control for semiconductor manufacturing

Der-Shui Lee · An-Chen Lee

Received: 11 June 2011 / Accepted: 4 July 2012 / Published online: 28 July 2012

Abstract This paper presents a new perspective on process control, called the two-dimensional pheromone propagation controller (2D-PPC), which considers the spatial information about disturbances of the process within a wafer to generate new predicted intercepts of the models for the subsequent use in time–effect controller (the exponentially weighted moving average, EWMA, in this study). The 2D-PPC assumes that the disturbances have their own behavior and affect others nearby in a wafer at a run; thus, it involves the "space-effect" among disturbances of the process at measurement positions within a wafer. The framework of the space–time controller (STC), which interlaces the time–effect controller and the space–effect 2D-PPC is constructed, and the stability analysis and intrinsic characteristics of the STC are discussed. Simulations are conducted using two-dimensional anthropogenic disturbances generated from fabrication data. The results show that the STC has better performance as compared to the conventional time–effect controllers. From implementation view point, since STC does not change the original code of time–effect controller, it can be easily implemented in the current process control loop by only adding an additional space-effect controller.

Keywords Two-dimensional pheromone propagation controller · Process control · Space-effect controller · Two-dimensional digital pheromone infrastructure · EWMA

D.-S. Lee · A.-C. Lee (✉)
Department of Mechanical Engineering,
National Chiao Tung University,
1001 Ta-Hsueh Road,
Hsinchu City, Taiwan, People's Republic of China
e-mail: aclee@mail.nctu.edu.tw

1 Introduction

In semiconductor manufacturing, run-to-run (RtR) control adjusts the recipe slightly based on in-line measurements to even out disturbances. Statistical process control (SPC) [1] and the exponentially weighted moving average (EWMA) controller [2–8] are widely used in semiconductor RtR control. Predictor corrector control (PCC) [9, 10] and double EWMA control [11–14] also have been proposed to improve the performance of EWMA when dealing with drifting processes. Recently, the output disturbance observer structure which provides a unified framework for the EWMA, the double EWMA and PCC controller is presented. [15]. In addition to EWMA-based solvers, artificial neural networks [16–18], recursive least square technique [19], time series analysis [20], extended Kalman filter [21], and pheromone propagation controller (PPC) [22] are applied in the RtR control. Besides, multivariate SPC [23, 24], multivariate EWMA controller [25–27], and multivariate double EWMA (dEWMA) controller [28] were also developed. No matter what kind of methodology is used in the RtR control, some researchers condense measurements to output quality characteristics, such as uniformity of CVD process [1, 2, 16, 23], removal rate of CMP process [3, 11, 17, 18], uniformity of CMP process [11, 17, 25], critical dimension of photolithography process [8], etching rate of etch process [9, 19], aluminum deposition rate of aluminum sputter deposition process [15, 20–22], and deposition thickness of diffusion process [27], for the process control; others employ control loops for every measurements, such as over 9,000 control loops for Y-markshift of lithography overlay control [4]; and still the others just control "output quality characteristics" without clear definition [5–7, 10, 12–14, 24, 26, 28]. Nowadays RtR controllers employ the "time–effect" characteristics among observed process data to calculate the recipe for the next run, which means disturbance of

a wafer affecting the output quality characteristics at later runs is assumed. In other words, traditional RtR control employs performance indices along "time" axis and losses the spatial information among different measurements within a wafer for each run.

In this paper, we propose an algorithm that includes the "space–effect" among disturbances of the process at measurement positions within a wafer at a run. The concept comes from the observation that a disturbance of a wafer at certain location will affect its neighborhood area which may contain several measurement positions at a run. The new algorithm uses swarm intelligence by assuming that disturbance of the process at measurement position has their own behavior and affects others nearby within a wafer at a run. Because measurements within a wafer are a two-dimensional layout, our novel algorithm is called the two-dimensional pheromone propagation controller (2D-PPC). This study modifies the propagation-out ratio of digital pheromone infrastructure [22, 29] to achieve 2D-PPC. Under the two-dimensional digital pheromone infrastructure, the disturbances at different measurements within a wafer are modeled as a social insect colony. The interaction among disturbances is modeled by a propagation mechanism, which means that a measurement affects others nearby. Using 2D-PPC, new predicted intercepts of the models are generated for the subsequent use in time–effect controller (EWMA in this study).

The framework of the space–time controller (STC) is then constructed, which interlaces the time–effect controller and the space–effect 2D-PPC. For maximum coverage with minimum measurements, this study assumes that the wafer has M_2 measurements in the triangular coordinate (hexagonal grids) layout whose examples are shown in Fig. 1. The subscript 2 of M_2 means the "two-dimensional" layout. In Fig. 1, the arrow means that measurements affect others nearby. For easy interpretation, the authors employ triangular grids with M_2=12 in the rest of this study and the notations are shown in Fig. 2. In Fig. 2, measurements are divided into two circles; measurements 1–6 are in the outer circle and the others (7–12) are in the inner circle. Figure 3 shows the concept of time–effect and space–effect controllers. Figure 3 is the concepts of the STC, which combines the MIMO (inputs are N_2 recipes and outputs are M_2 measurement data) time–effect controller with 2D-PPC. In Fig. 3, after forecasting disturbances by the MIMO time–effect controller, the two-dimensional disturbances predictor, which is the realization of space–effect controller, modifies the forecasting disturbances of the MIMO time–effect controller spatially by 2D disturbances predictor for the next run. In other words, the STC interlaces time–effect and space–effects at a run and then the process recipe for the next run can be obtained by the forecast disturbances.

The stability analysis of the STC shows that larger stability region is obtained as compared to the MIMO time–effect controller. Also, simulations are conducted to compare the output performance of three MIMO time–effect controllers, EWMA, PCC, and dEWMA, with and without 2D-PPC. The two-dimensional anthropogenic disturbances are generated from fabrication data of CMP process and the candidate controllers are examined by sum square error (SSE) in the simulation study. The simulation results show that the STC improves the output performance as compared to the MIMO time–effect controllers.

The rest of this paper is organized as follows. Section 2 conducts the two-dimensional digital pheromone infrastructure. Section 3 illustrates the STC structure. Section 4 analyzes the STC stability region and compares the intrinsic properties of STC with those of the time–effect controller. Section 5 shows the simulation results for the proposed controller. The final section draws the conclusion.

2 The two-dimensional digital pheromone infrastructure

The concept of the space–effect 2D-PPC comes from the appearance that a disturbance of the process at a measurement position in a wafer will be affected by its nearby disturbances at measurement positions within the same wafer at a run and the space–effect will maintain to affect the next wafer in semiconductor fabrication. Corresponding to the food trail pheromones or alarm pheromones in the nature, the 2D-PPC employs "disturbance pheromones" within the same wafer at a run in the manufacturing process. The 2D-PPC is an extension of PPC [22] and the digital pheromone infrastructures of PPC and 2D-PPC only differ from the shape of pheromone basket and the propagation-out ratio of transition

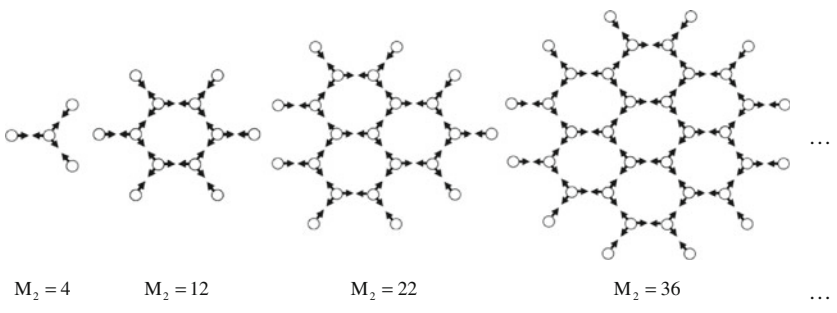

Fig. 1 Examples of M_2 measurements in triangular coordinate (hexagonal grids) layout

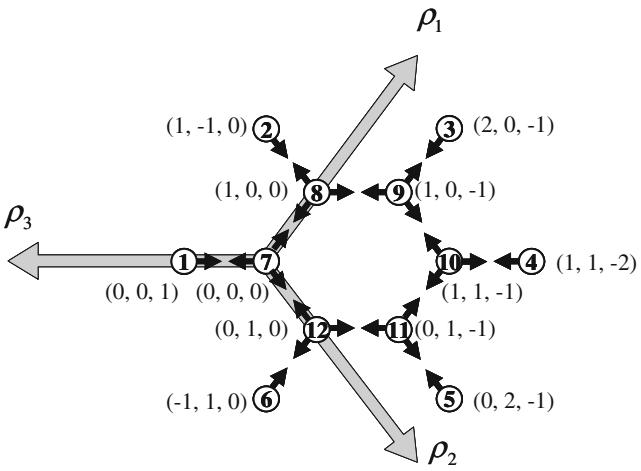

Fig. 2 Layout of the 12 measurement positions within a wafer

functions. This section will introduce the two-dimensional digital pheromone infrastructure which includes pheromone basket, pheromone states, transition parameters and transition functions.

2.1 Pheromone basket

The pheromone basket is the pheromone propagation environment. The "two-dimensional" PPC is named by the fact that the shape of pheromone basket is a two-dimensional plane. The environment of two-dimensional digital pheromone infrastructure is a tuple $<B, N>$, where B is a finite set of positions $b_{m_2} \in B : m_2 = 1, 2, \ldots, \mathrm{M}_2$ within the pheromone basket with size M_2. Specifically, b_{m_2} of 2D-PPC maps the measurement position in the wafer. Then, $N(b_{m_2}) \subseteq B$ is a finite set of neighbors of b_{m_2} and $|N(b_{m_2})|$ is the size of $N(b_{m_2})$. Suppose that (ρ_1, ρ_2, ρ_3) in Fig. 2 is the triangular coordinate (hexagonal grids) of position b_{m_2} in the two-dimensional digital space [30], the coordinate of $N(b_{m_2})$ is $(\rho_1', \rho_2', \rho_3')$, where

$$\begin{cases} |\rho_1' - \rho_1| \le 1 \\ |\rho_2' - \rho_2| \le 1 \\ |\rho_3' - \rho_3| \le 1 \\ |\rho_1' - \rho_1| + |\rho_2' - \rho_2| + |\rho_3' - \rho_3| = 1 \end{cases} \quad (1)$$

In addition, the two-dimensional digital pheromone infrastructure assumes that the propagation relationship between $N(b_{m_2})$ and b_{m_2} is irreflective, which means that b_{m_2} will accept propagation inputs from $N(b_{m_2})$ without preconditions.

The pheromone basket is initially empty, and then filled with M_2 disturbances within the same wafer at each time stamp (or run). In other words, the disturbances within a wafer can be treated as the external impulse input to the two-dimensional pheromone basket. The external input of two-dimensional pheromone basket is a finite set $R_2(k, i) = \{r_2(k, b_{m_2}, i) \in (-L, L) : m_2 = 1, 2, \ldots, M_2\}$, where k=1, 2, …, is the run number of the manufacturing process, $i \in \aleph$ is the number of iterations (or propagations) in the transition functions, and $L \in \Re$ is the global limit of the external inputs in the environment $<B, N>$. We use the notation $\aleph$ for the set of natural numbers and $\Re$ for the set of real numbers. Since the external input is the initial condition for launching transition functions of pheromone propagation, $r_2(k, b_{m_2}, 0)$ maps to the disturbances at position b_{m_2} at the run k and $r_2(k, b_{m_2}, i)$ is 0 when i is larger than 0.

2.2 Pheromone states

Like [22, 29], the states in the two-dimensional pheromone basket $<B, N>$ are $Q_2(k, i)$ and $S_2(k, i)$, where $Q_2(k, i) = \{q_2(k, b_{m_2}, i) \in \Re : m_2 = 1, 2, \ldots, \mathrm{M}_2\}$ is a finite set of the propagated inputs at run k and iteration i, and $S_2(k, i) = \{s_2(k, b_{m_2}, i) \in \Re : m_2 = 1, 2, \ldots, \mathrm{M}_2\}$ is a

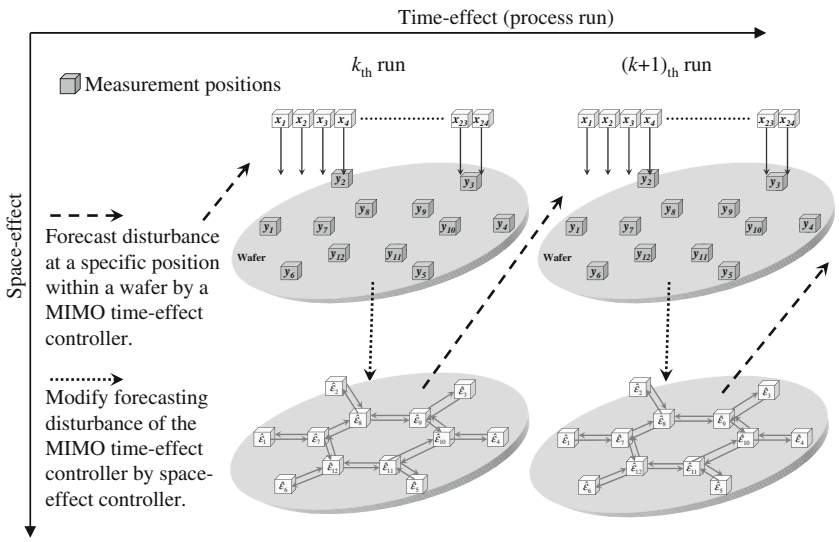

Fig. 3 Concept of STC, which combines MIMO (M_2=12 and N_2=24 in this example) time–effect controller and space–effect (2D-PPC) controller, where $x_1, x_2, \cdots x_{N_2}$ are recipes, $y_1, y_2, \cdots y_{\mathrm{M}_2}$ are measurement outputs and $\widehat{\varepsilon}_1, \widehat{\varepsilon}_2, \cdots \widehat{\varepsilon}_{\mathrm{M}_2}$ are the forecasting disturbances

finite set of the aggregated pheromones at run k and iteration i. Therefore, $q_2(k, b_{m_2}, i)$ is regarded as the propagated input from $N(b_{m_2})$ to b_{m_2} at iteration i and run k. Similarly, $s_2(k, b_{m_2}, i)$ is regarded as the aggregated pheromone of b_{m_2} at iteration i and run k.

In addition, $q_2(k, b_{m_2}, 0) = 0$ and $s_2(k, b_{m_2}, 0) = 0$ are assumed to be the default initial conditions. While launching transition functions as shown in the following sections, $Q_2(k, i)$ disseminates pheromones and $S_2(k, i)$ aggregates pheromones simultaneously.

2.3 Pheromone transition parameters

By [22, 29], two transition parameters of the two-dimensional digital pheromone infrastructure are the evaporation parameter $E_2 \in (0,1]$ and the propagation parameter $F_2 \in [0,1)$. In 2D-PPC, the propagation parameter F_2 describes the effect of disturbance of the process on other nearby disturbance within the same wafer, and the evaporation parameter E_2 indicates that the importance of the measurement data will "evaporate" with time. Because measurements within a chamber at a time stamp can be treated as a nondissipative system, the modified pheromone infrastructure uses $E_2=1$ [22].

2.4 Transition functions

With the introduction of the two-dimensional pheromone basket $<B, N>$, the parameters E_2 and F_2, the external input $R_2(k, i)$, states $Q_2(k, i)$ and $S_2(k, i)$, transition functions of 2D-PPC can be developed. This section will modify the propagation-out ratio of transition functions in digital pheromone infrastructure [22] to erase the boundary effect of a plane pheromone basket.

The propagation-out ratio at the frontier points of Fig. 2 needs to be modified from $F_2/(2-F_2)$ [22] to $F_2/(3-2F_2)$ (proof is given in Appendix A). Then, the transition functions become

$$q_2(k, b_{m_2}, i+1) = \begin{cases} \frac{F_2}{3}(r_2(k, b_{m_2+6}, i) + q_2(k, b_{m_2+6}, i)), & \text{if} m_2 = 1, 2, \ldots, 6 \\ \frac{F_2}{3-2F_2}(r_2(k, b_{m_2-6}, i) + q_2(k, b_{m_2-6}, i)) + \frac{F_2}{3}(r_2(k, b_{m_2+1}, i) + q_2(k, b_{m_2+1}, i)) & \\ \quad + \frac{F_2}{3}(r_2(k, b_{m_2-1}, i) + q_2(k, b_{m_2-1}, i)), & \text{if} m_2 = 8, 9, \ldots, 11 \\ \frac{F_2}{3-2F_2}(r_2(k, b_{m_2-6}, i) + q_2(k, b_{m_2-6}, i)) + \frac{F_2}{3}(r_2(k, b_{m_2+1}, i) + q_2(k, b_{m_2+1}, i)) & \\ \quad + \frac{F_2}{3}(r_2(k, b_{12}, i) + q_2(k, b_{12}, i)), & \text{if} m_2 = 7 \\ \frac{F_2}{3-2F_2}(r_2(k, b_{m_2-6}, i) + q_2(k, b_{m_2-6}, i)) + \frac{F_2}{3}(r_2(k, b_7, i) + q_2(k, b_7, i)) & \\ \quad + \frac{F_2}{3}(r_2(k, b_{m_2-1}, i) + q_2(k, b_{m_2-1}, i)), & \text{if} m_2 = 12 \end{cases} \tag{2}$$

$$s_2(k, b_{m_2}, i+1) = \begin{cases} s_2(k, b_{m_2}, i) + \left(1 - \frac{F_2}{3-2F_2}\right)(r_2(k, b_{m_2}, i) + q_2(k, b_{m_2}, i)), & \text{if } m_2 = 1, 2, ..., 6. \\ s_2(k, b_{m_2}, i) + (1-F_2)(r_2(k, b_{m_2}, i) + q_2(k, b_{m_2}, i)), & \text{if } m_2 = 7, 8, \ldots, 12. \end{cases} \tag{3}$$

Figure 4 illustrates the concept of Eqs. 2 and 3. In fact, one can apply transition functions in Cartesian coordinate system by modifying the propagation-out ratio from $F_2/(3-2F_2)$ to $F_2/(4-3F_2)$ in Eqs. 2 and 3 by same procedure in Appendix A. Then, the final propagation results of Eqs. 2 and 3 can be obtained by Eq. (A.8) in the Appendix B. For example, if M_2 is 12, the final propagation results at b_{m_2} is

$$s_2(k, b_{m_2}, \infty) = \begin{bmatrix} P_{2,1,m_2} \\ P_{2,2,m_2} \\ \vdots \\ P_{2,12,m_2} \end{bmatrix}^{\mathrm{T}} \begin{bmatrix} r_2(k, b_1, 0) \\ r_2(k, b_2, 0) \\ \vdots \\ r_2(k, b_{12}, 0) \end{bmatrix}, \quad m_2 = 1, 2, \ldots, 12. \tag{4}$$

where $P_{2,1,m_2}, P_{2,2,m_2}, \ldots,$ and $P_{2,12,m_2}$ are the quantity of positions 1–12 affecting position b_{m_2} within the two-dimensional pheromone basket and the values of $P_{2,1,m_2}$, $P_{2,2,m_2}, \ldots,$ and $P_{2,12,m_2}$ are listed at no. 1–12 of Table 1.

3 Space–time controller

The STC interlaces the time–effect controller, such as EWMA or PCC and so on, with the space–effect controller, 2D-PPC, in pairs. Figure 5 is the scalar-form block diagram of EWMA with 2D-PPC when the layout of measurements is like Fig. 2. In Fig. 5, the control loop of STC (EWMA with 2D-PPC) can be separated into four modules: MIMO plant, the time–effect controller, the space–effect controller and MIMO recipe generator. Sections 3.1 to 3.4 describe each of these modules.

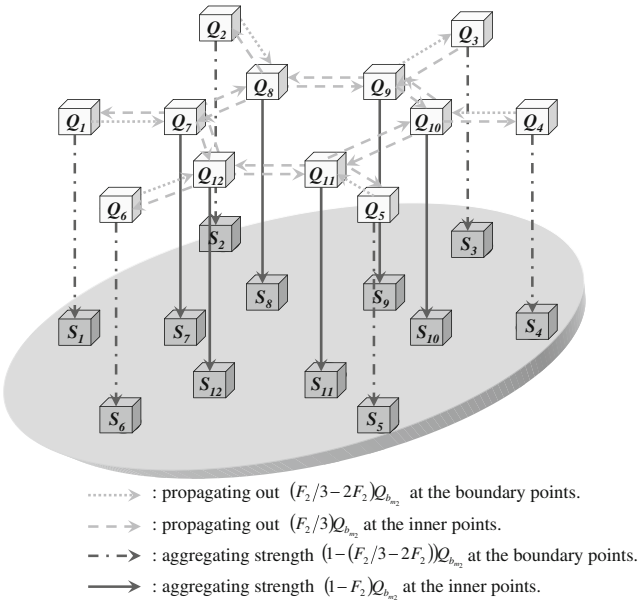

Fig. 4 Transitions with propagation parameter F_2 and size $M_2=12$ in a two-dimensional pheromone basket

3.1 MIMO plant

The linear regression model is assumed for the process model. Based on twelve measurements as in Fig. 2, this study assumes the process has 12 outputs and each output has its own disturbance, process gain and two inputs. The demonstrated MIMO plant is

$$\mathbf{Y_{k+1}} = \alpha + \beta \cdot \mathbf{X_k} + \varepsilon_{\mathbf{k+1}} \quad k = 0, 1, 2, \ldots, \tag{5}$$

where

$$\mathbf{Y_{k+1}} = [\, Y_{1,k+1} \quad Y_{2,k+1} \quad \cdots \quad Y_{m_2,k+1} \quad \cdots \quad Y_{\mathrm{M}_2,k+1} \,]^{\mathrm{T}},$$

$$\mathbf{X_k} = [\, X_{1,k} \quad X_{2,k} \quad \cdots \quad X_{n_2,k} \quad \cdots \quad X_{\mathrm{N}_2,k} \,]^{\mathrm{T}},$$

$$\alpha = [\, \alpha_1 \quad \alpha_2 \quad \cdots \quad \alpha_{m_2} \quad \cdots \quad \alpha_{\mathrm{M}_2} \,]^{\mathrm{T}},$$

$$\beta = \begin{bmatrix} \beta_{1,1} & \beta_{1,2} & \cdots & \beta_{1,n_2} & \cdots & \beta_{1,\mathrm{N}_2} \\ \beta_{2,1} & \beta_{2,2} & \cdots & \beta_{2,n_2} & \cdots & \beta_{2,\mathrm{N}_2} \\ \vdots & \vdots & \ddots & \vdots & \vdots & \vdots \\ \beta_{m_2,1} & \beta_{m_2,2} & \cdots & \beta_{m_2,n_2} & \cdots & \beta_{m_2,\mathrm{N}_2} \\ \vdots & \vdots & \cdots & \vdots & \ddots & \vdots \\ \beta_{\mathrm{M}_2,1} & \beta_{\mathrm{M}_2,2} & \cdots & \beta_{\mathrm{M}_2,n_2} & \cdots & \beta_{\mathrm{M}_2,\mathrm{N}_2} \end{bmatrix}, \text{ and}$$

$$\varepsilon_{\mathbf{k+1}} = [\, \varepsilon_{1,k+1} \quad \varepsilon_{2,k+1} \quad \cdots \quad \varepsilon_{m_2,k+1} \quad \cdots \quad \varepsilon_{\mathrm{M}_2,k+1} \,]^{\mathrm{T}}.$$

In addition,

$Y_{1,k}, Y_{2,k}, \cdots, Y_{\mathrm{M}_2,k} \in \Re$	M_2 measurements at the end of run k
$X_{1,k}, X_{2,k}, \cdots, X_{\mathrm{N}_2,k} \in \Re$	N_2 recipes (inputs) of a wafer at run k
$\alpha_1, \alpha_2, \cdots, \alpha_{\mathrm{M}_2} \in \Re$	intercepts of the process
$\beta_{1,1}, \beta_{1,2}, \cdots, \beta_{\mathrm{M}_2,\mathrm{N}_2} \in \Re$	system gains
$\varepsilon_{1,k}, \varepsilon_{2,k}, \cdots, \varepsilon_{\mathrm{M}_2,k} \in \Re$	disturbances, which include noise and uncontrolled terms of run k.

3.2 The time–effect controller

The MIMO time–effect controller is a traditional controller, such as MIMO EWMA, MIMO dEWMA, MIMO PCC, and so on, applied to all measurement positions within a wafer. Since MIMO EWMA is now commonly used in semiconductor fabrication, this study employs it as a demonstrated MIMO time–effect controller and the forecast disturbance of the MIMO EWMA controller at run $k+1$, $\widetilde{\varepsilon}_{\mathbf{k+1}}$, becomes

$$\begin{aligned} \widetilde{\varepsilon}_{\mathbf{k+1}} &= [\, \widetilde{\varepsilon}_{1,k+1} \quad \widetilde{\varepsilon}_{2,k+1} \quad \cdots \quad \widetilde{\varepsilon}_{m_2,k+1} \quad \cdots \quad \widetilde{\varepsilon}_{\mathrm{M}_2,k+1} \,]^{\mathrm{T}} \\ &= \Lambda\left(\mathbf{Y_k} - \alpha - \widehat{\beta}\mathbf{X_k}\right) + (\mathbf{I} - \Lambda)\widetilde{\varepsilon}_{\mathbf{k}} \end{aligned} \tag{6}$$

where $\Lambda = \lambda\mathbf{I}$ is the discount factor of MIMO EWMA. The Eq. (6) can be applied both in $M_2 \geq N_2$ and $M_2 \leq N_2$.

3.3 The space–effect controller

The infrastructure of the space–effect controller has described in Section 2. Then, the input of 2D pheromone basket is the forecasting disturbances of the MIMO time–effect controller.

$$\mathbf{R_2}(k,0) = \begin{bmatrix} r_2(k,b_1,0) \\ r_2(k,b_2,0) \\ \vdots \\ r_2(k,b_{m_2},0) \\ \vdots \\ r_2(k,b_{\mathrm{M}_2},0) \end{bmatrix} = \begin{bmatrix} \widetilde{\varepsilon}_{1,k+1} \\ \widetilde{\varepsilon}_{2,k+1} \\ \vdots \\ \widetilde{\varepsilon}_{m_2,k+1} \\ \vdots \\ \widetilde{\varepsilon}_{\mathrm{M}_2,k+1} \end{bmatrix} \tag{7}$$

And the forecast disturbance of 2D-PPC at run $k+1$, $\hat{\varepsilon}_{\mathbf{k+1}}$, can be obtained by substituting Eq. (7) into Eq. (4).

$$\widehat{\varepsilon}_{\mathbf{k+1}} = \begin{bmatrix} \widehat{\varepsilon}_{1,k+1} \\ \widehat{\varepsilon}_{2,k+1} \\ \vdots \\ \widehat{\varepsilon}_{m_2,k+1} \\ \vdots \\ \widehat{\varepsilon}_{\mathrm{M}_2,k+1} \end{bmatrix} = \begin{bmatrix} P_{2,1,1} & P_{2,2,1} & \cdots & P_{2,m_2,1} & \cdots & P_{2,\mathrm{M}_2,1} \\ P_{2,1,2} & P_{2,2,2} & \cdots & P_{2,m_2,2} & \cdots & P_{2,\mathrm{M}_2,2} \\ \vdots & \vdots & \ddots & & & \vdots \\ P_{2,1,m_2} & P_{2,2,m_2} & & P_{2,m_2,m_2} & & P_{2,\mathrm{M}_2,m_2} \\ \vdots & \vdots & & & \ddots & \vdots \\ P_{2,1,\mathrm{M}_2} & P_{2,2,\mathrm{M}_2} & \cdots & P_{2,m_2,\mathrm{M}_2} & \cdots & P_{2,\mathrm{M}_2,\mathrm{M}_2} \end{bmatrix} \begin{bmatrix} \widetilde{\varepsilon}_{1,k+1} \\ \widetilde{\varepsilon}_{2,k+1} \\ \vdots \\ \widetilde{\varepsilon}_{m_2,k+1} \\ \vdots \\ \widetilde{\varepsilon}_{\mathrm{M}_2,k+1} \end{bmatrix} \tag{8}$$

Table 1 Notations and values of Eqs. (4), (8), and (13)

No.	Notation	Value
1	$P_{2,1,1}$, $P_{2,2,2}$, $P_{2,3,3}$, $P_{2,4,4}$, $P_{2,5,5}$, $P_{2,6,6}$	$\frac{28\widehat{F}^7_{2,k+1}-219\widehat{F}^6_{2,k+1}+162\widehat{F}^5_{2,k+1}+1566\widehat{F}^4_{2,k+1}-2754\widehat{F}^3_{2,k+1}-972\widehat{F}^2_{2,k+1}+4374\widehat{F}_{2,k+1}-2187}{3\left(5\widehat{F}^7_{2,k+1}-55\widehat{F}^6_{2,k+1}+96\widehat{F}^5_{2,k+1}+324\widehat{F}^4_{2,k+1}-864\widehat{F}^3_{2,k+1}+1215\widehat{F}_{2,k+1}-729\right)}$
2	$P_{2,2,1}$, $P_{2,6,1}$, $P_{2,1,2}$, $P_{2,3,2}$, $P_{2,2,3}$, $P_{2,4,3}$, $P_{2,3,4}$, $P_{2,5,4}$, $P_{2,4,5}$, $P_{2,6,5}$, $P_{2,1,6}$, $P_{2,5,6}$	$\frac{7\widehat{F}^7_{2,k+1}-36\widehat{F}^6_{2,k+1}+108\widehat{F}^4_{2,k+1}-81\widehat{F}^3_{2,k+1}}{3\left(5\widehat{F}^7_{2,k+1}-55\widehat{F}^6_{2,k+1}+96\widehat{F}^5_{2,k+1}+324\widehat{F}^4_{2,k+1}-864\widehat{F}^3_{2,k+1}+1215\widehat{F}_{2,k+1}-729\right)}$
3	$P_{2,3,1}$, $P_{2,5,1}$, $P_{2,4,2}$, $P_{2,6,2}$, $P_{2,1,3}$, $P_{2,5,3}$, $P_{2,2,4}$, $P_{2,6,4}$, $P_{2,1,5}$, $P_{2,3,5}$, $P_{2,2,6}$, $P_{2,4,6}$,	$\frac{-2\widehat{F}^7_{2,k+1}-9\widehat{F}^6_{2,k+1}+36\widehat{F}^5_{2,k+1}-27\widehat{F}^4_{2,k+1}}{3\left(5\widehat{F}^7_{2,k+1}-55\widehat{F}^6_{2,k+1}+96\widehat{F}^5_{2,k+1}+324\widehat{F}^4_{2,k+1}-864\widehat{F}^3_{2,k+1}+1215\widehat{F}_{2,k+1}-729\right)}$
4	$P_{2,4,1}$, $P_{2,5,2}$, $P_{2,6,3}$, $P_{2,1,4}$, $P_{2,2,5}$, $P_{2,3,6}$,	$\frac{-8\widehat{F}^7_{2,k+1}+24\widehat{F}^6_{2,k+1}-18\widehat{F}^5_{2,k+1}}{3\left(5\widehat{F}^7_{2,k+1}-55\widehat{F}^6_{2,k+1}+96\widehat{F}^5_{2,k+1}+324\widehat{F}^4_{2,k+1}-864\widehat{F}^3_{2,k+1}+1215\widehat{F}_{2,k+1}-729\right)}$
5	$P_{2,7,1}$, $P_{2,8,2}$, $P_{2,9,3}$, $P_{2,10,4}$, $P_{2,11,5}$, $P_{2,12,6}$, $P_{2,1,7}$, $P_{2,2,8}$, $P_{2,3,9}$, $P_{2,4,10}$, $P_{2,5,11}$, $P_{2,6,12}$,	$\frac{-11\widehat{F}^7_{2,k+1}-18\widehat{F}^6_{2,k+1}+378\widehat{F}^5_{2,k+1}-594\widehat{F}^4_{2,k+1}-486\widehat{F}^3_{2,k+1}+1458\widehat{F}^2_{2,k+1}-729\widehat{F}_{2,k+1}}{3(5\widehat{F}^7_{2,k+1}-55\widehat{F}^6_{2,k+1}+96\widehat{F}^5_{2,k+1}+324\widehat{F}^4_{2,k+1}-864\widehat{F}^3_{2,k+1}+1215F_{2,k+1}-729)}$
6	$P_{2,8,1}$, $P_{2,12,1}$, $P_{2,7,2}$, $P_{2,9,2}$, $P_{2,8,3}$, $P_{2,10,3}$, $P_{2,9,4}$, $P_{2,11,4}$, $P_{2,10,5}$, $P_{2,12,5}$, $P_{2,7,6}$, $P_{2,11,6}$, $P_{2,2,7}$, $P_{2,6,7}$, $P_{2,1,8}$, $P_{2,3,8}$, $P_{2,2,9}$, $P_{2,4,9}$, $P_{2,3,10}$, $P_{2,5,10}$, $P_{2,4,11}$, $P_{2,6,11}$, $P_{2,1,12}$, $P_{2,5,12}$,	$\frac{-14\widehat{F}^7_{2,k+1}+93\widehat{F}^6_{2,k+1}-108\widehat{F}^5_{2,k+1}-216\widehat{F}^4_{2,k+1}+486\widehat{F}^3_{2,k+1}-243\widehat{F}^2_{2,k+1}}{3\left(5\widehat{F}^7_{2,k+1}-55\widehat{F}^6_{2,k+1}+96\widehat{F}^5_{2,k+1}+324\widehat{F}^4_{2,k+1}-864\widehat{F}^3_{2,k+1}+1215\widehat{F}_{2,k+1}-729\right)}$
7	$P_{2,9,1}$, $P_{2,11,1}$, $P_{2,10,2}$, $P_{2,12,2}$, $P_{2,7,3}$, $P_{2,11,3}$, $P_{2,8,4}$, $P_{2,12,4}$, $P_{2,7,5}$, $P_{2,9,5}$, $P_{2,8,6}$, $P_{2,10,6}$, $P_{2,3,7}$, $P_{2,5,7}$, $P_{2,4,8}$, $P_{2,6,8}$, $P_{2,1,9}$, $P_{2,5,9}$, $P_{2,2,10}$, $P_{2,6,10}$, $P_{2,1,11}$, $P_{2,3,11}$, $P_{2,2,12}$, $P_{2,4,12}$,	$\frac{4\widehat{F}^7_{2,k+1}+12\widehat{F}^6_{2,k+1}-99\widehat{F}^5_{2,k+1}+162\widehat{F}^4_{2,k+1}-81\widehat{F}^3_{2,k+1}}{3\left(5\widehat{F}^7_{2,k+1}-55\widehat{F}^6_{2,k+1}+96\widehat{F}^5_{2,k+1}+324\widehat{F}^4_{2,k+1}-864\widehat{F}^3_{2,k+1}+1215\widehat{F}_{2,k+1}-729\right)}$
8	$P_{2,10,1}$, $P_{2,11,2}$, $P_{2,12,3}$, $P_{2,7,4}$, $P_{2,8,5}$, $P_{2,9,6}$, $P_{2,4,7}$, $P_{2,5,8}$, $P_{2,6,9}$, $P_{2,1,10}$, $P_{2,2,11}$, $P_{2,3,12}$,	$\frac{16\widehat{F}^7_{2,k+1}-72\widehat{F}^6_{2,k+1}+108\widehat{F}^5_{2,k+1}-54\widehat{F}^4_{2,k+1}}{3\left(5\widehat{F}^7_{2,k+1}-55\widehat{F}^6_{2,k+1}+96\widehat{F}^5_{2,k+1}+324\widehat{F}^4_{2,k+1}-864\widehat{F}^3_{2,k+1}+1215\widehat{F}_{2,k+1}-729\right)}$
9	$P_{2,7,7}$, $P_{2,8,8}$, $P_{2,9,9}$, $P_{2,10,10}$, $P_{2,11,11}$, $P_{2,12,12}$,	$\frac{22\widehat{F}^7_{2,k+1}+3\widehat{F}^6_{2,k+1}-810\widehat{F}^5_{2,k+1}+2322\widehat{F}^4_{2,k+1}-810\widehat{F}^3_{2,k+1}-4374\widehat{F}^2_{2,k+1}+5832\widehat{F}_{2,k+1}-2187}{3\left(5\widehat{F}^7_{2,k+1}-55\widehat{F}^6_{2,k+1}+96\widehat{F}^5_{2,k+1}+324\widehat{F}^4_{2,k+1}-864\widehat{F}^3_{2,k+1}+1215\widehat{F}_{2,k+1}-729\right)}$
10	$P_{2,8,7}$, $P_{2,12,7}$, $P_{2,7,8}$, $P_{2,9,8}$, $P_{2,8,9}$, $P_{2,10,9}$, $P_{2,9,10}$, $P_{2,11,10}$, $P_{2,10,11}$, $P_{2,12,11}$, $P_{2,7,12}$, $P_{2,11,12}$	$\frac{28\widehat{F}^7_{2,k+1}-228\widehat{F}^6_{2,k+1}+495\widehat{F}^5_{2,k+1}+108\widehat{F}^4_{2,k+1}-1620\widehat{F}^3_{2,k+1}+1944\widehat{F}^2_{2,k+1}-729\widehat{F}_{2,k+1}}{3\left(5\widehat{F}^7_{2,k+1}-55\widehat{F}^6_{2,k+1}+96\widehat{F}^5_{2,k+1}+324\widehat{F}^4_{2,k+1}-864\widehat{F}^3_{2,k+1}+1215\widehat{F}_{2,k+1}-729\right)}$
11	$P_{2,9,7}$, $P_{2,11,7}$, $P_{2,10,8}$, $P_{2,12,8}$, $P_{2,7,9}$, $P_{2,11,9}$, $P_{2,8,10}$, $P_{2,12,10}$, $P_{2,7,11}$, $P_{2,9,11}$, $P_{2,8,12}$, $P_{2,10,12}$	$\frac{-8\widehat{F}^7_{2,k+1}-12\widehat{F}^6_{2,k+1}+234\widehat{F}^5_{2,k+1}-621\widehat{F}^4_{2,k+1}+648\widehat{F}^3_{2,k+1}-243\widehat{F}^2_{2,k+1}}{3\left(5\widehat{F}^7_{2,k+1}-55\widehat{F}^6_{2,k+1}+96\widehat{F}^5_{2,k+1}+324\widehat{F}^4_{2,k+1}-864\widehat{F}^3_{2,k+1}+1215\widehat{F}_{2,k+1}-729\right)}$
12	$P_{2,10,7}$, $P_{2,11,8}$, $P_{2,12,9}$, $P_{2,7,10}$, $P_{2,8,11}$, $P_{2,9,12}$	$\frac{-32\widehat{F}^7_{2,k+1}+192\widehat{F}^6_{2,k+1}-432\widehat{F}^5_{2,k+1}+432\widehat{F}^4_{2,k+1}-162\widehat{F}^3_{2,k+1}}{3(5\widehat{F}^7_{2,k+1}-55\widehat{F}^6_{2,k+1}+96\widehat{F}^5_{2,k+1}+324\widehat{F}^4_{2,k+1}-864\widehat{F}^3_{2,k+1}+1215\widehat{F}_{2,k+1}-729)}$
13	G_1, G_2, …, G_{12}	1
14	$G_{25,13}$, $G_{26,14}$, …, $G_{36,24}$	1
15	$G_{25,1}$, $G_{26,2}$, …, $G_{36,12}$	−1
16	W_1, W_2, …, W_{12}	$-\lambda/(\mathrm{z}+\lambda-1)$
17	$G_{\mathrm{i},\ \mathrm{j}+24}$, where i=1, 2, …, 12 and j=1, 2, …, 12.	$W_{\mathrm{j}}.P_{2,\mathrm{j},\mathrm{i}}$, where i=1, 2, … 12 and j=1, 2, …, 12

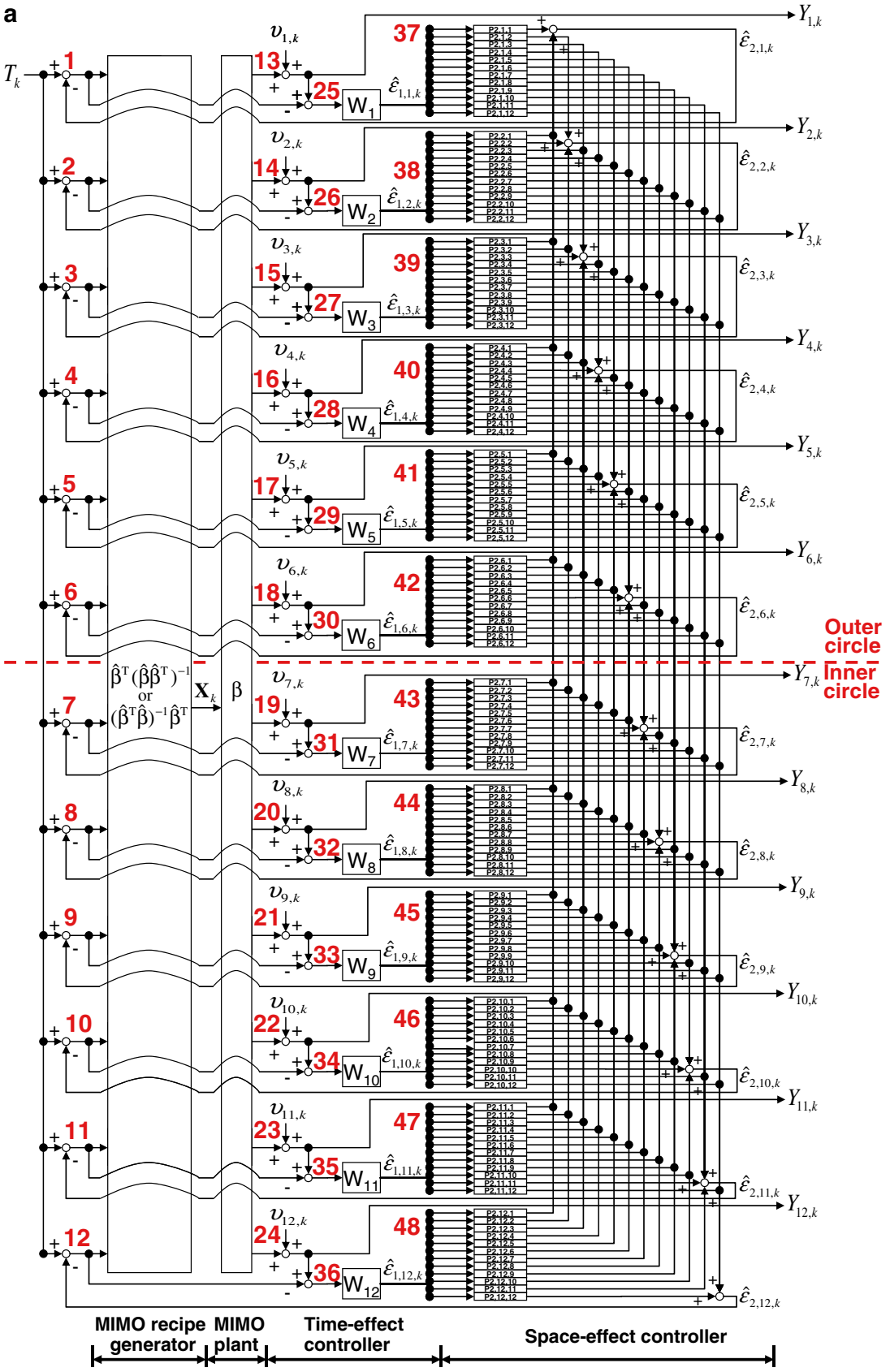

Fig. 5 Scalar form block diagram of a STC using EWMA as a time-effect controller with measurements layout in Fig. 1 and plant in Section 3.1. **a** Block diagram. **b** Details of nodes 37-48 in Fig. 5a

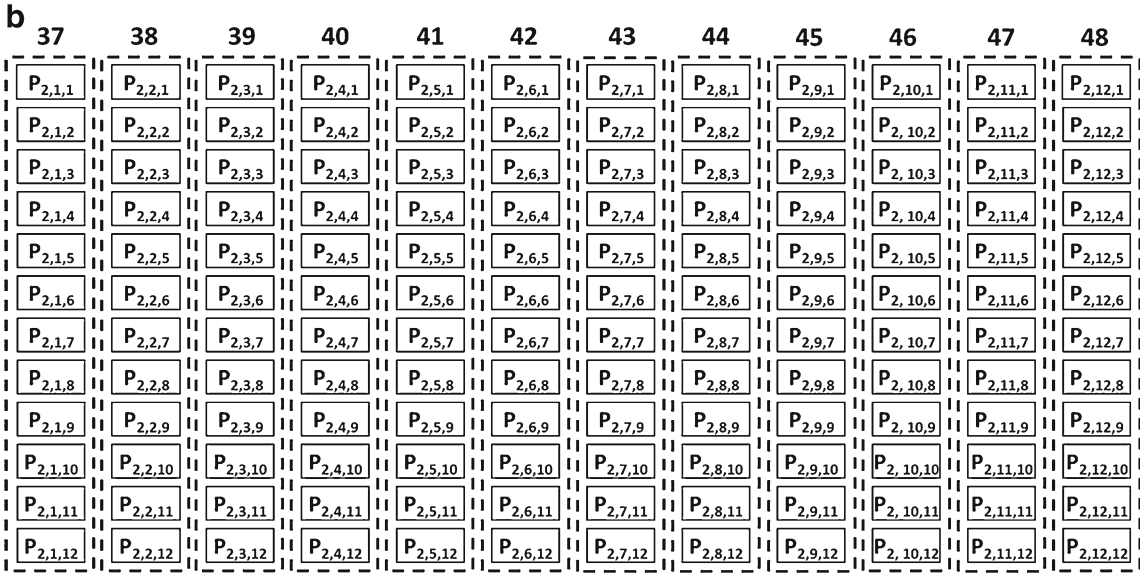

Fig. 5 (continued)

where the values of $P_{2,1,1}$, $P_{2,2,1}$, …, and P_{2,M_2,M_2} are listed at no. 1–12 of Table 1.

Figure 6a–f show an example of propagation results with different 2D propagation parameters F_2 for a two-dimensional pheromone basket in Fig. 2. Figure 6a is the external inputs initially, and Fig. 6b–f illustrate the final propagation results with different F_2. If F_2 is 0, the space–effect controller does not modify the forecasting disturbances of the MIMO time–effect controller, i.e., the 2D-PPC is disable. In addition, the propagation

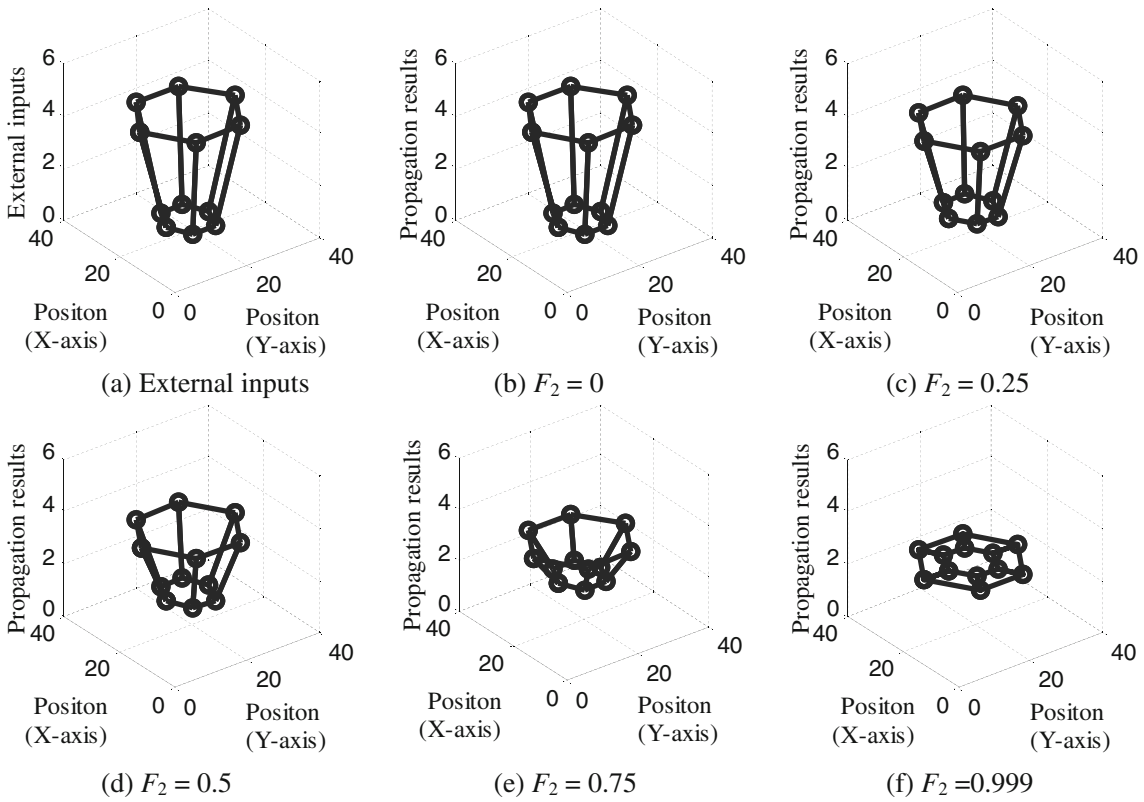

Fig. 6 An example of different propagation results with different 2D propagation parameters F_2 for a two-dimensional pheromone basket shown in Fig. 2

result approaches the mean of the external inputs as F_2 approaches unity.

3.4 MIMO recipe generator

The recipe generator generates the recipe of the process for the next run. In Fig. 5, we use the linear regression model to produce

$$\mathbf{T} = \widehat{\alpha} + \widehat{\beta} \cdot \mathbf{X_{k+1}} + \widehat{\varepsilon}_{\mathbf{k+1}}, \tag{9}$$

where $\mathbf{X}_{k+1}$ is the recipe (input) of run $k+1$, $\widehat{\alpha}$ is the estimator of the intercept α, $\widehat{\beta}$ is the estimator of the system β *and* $\mathbf{T} = [\,T \quad T \quad \cdots \quad T\,]^{\mathrm{T}}_{1\times \mathrm{M}_2}$ is a given target values of measurements within a wafer. The recipe for run $k+1$, $\mathbf{X}_{k+1}$, is given based on different conditions:

1. If $M_2 \geq N_2$,

$$\mathbf{X}_{k+1} = \left(\widehat{\beta}^T\widehat{\beta}\right)^{-1}\widehat{\beta}^T(\mathbf{T} - \widehat{\alpha} - \widehat{\varepsilon}_{k+1}) \tag{10}$$

(2) If $M_2 \leq N_2$,

$$\mathbf{X}_{k+1} = \widehat{\beta}^T\left(\widehat{\beta}\widehat{\beta}^T\right)^{-1}(\mathbf{T} - \widehat{\alpha} - \widehat{\varepsilon}_{k+1}) \tag{11}$$

(3) If $M_2 = N_2$,

One selects Eq. (10) to minimize the sum of the manipulated variables squared or Eq. (11) to minimize the sum of squares deviation from target [13].

In addition, $\widehat{\alpha}$ and $\widehat{\beta}$ in Eqs. (10) and (11) are obtained from the linear regression model of the offline data and the parameter $\widehat{\varepsilon}_{k+1}$ comes from Eq. (8).

3.5 The controller parameter tuners

The controller parameters of STC are the EWMA discount factors, λ, in Eq. (6) and the 2D propagation parameter, F_2, in Eq. (8). The best controller parameters can be obtained by using historical (or training) data and examining all possible values of controller parameters. In this study, we utilized the ordinary tuning method of the traditional time–effect controller to obtain a set of the best propagation parameter $\overline{F}_2$, and discount factors, $\overline{\lambda}_{\overline{F}_2}$, of the time–effect controller for $\overline{F}_2$ by minimum sum square error, or

$$\left(\overline{F}_2, \overline{\lambda}_{\overline{F}_2}\right) \cong \min_{F_2, \lambda_{F_2}} \left(\sum_{m_2}\sum_{k'} e^2_{m_2,k'}\right) \tag{12}$$

where $e^2_{m_2,k'}$ is error at position m_2 and the k'th training data.

3.6 Control procedure

The STC interlaces the space–effect 2D-PPC and the time–effect controller in pairs. In this section, the control procedure of STC is presented in the following sequence:

Step 1 Run time–effect controller, such as MIMO EWMA in Eq. (6) with the discount factor, $\overline{\lambda}_{\overline{F}_2}$, obtained from Eq. (12) at first two runs and obtain process error $\mathbf{e}_k$, where k=1 and 2. Then do follow-up steps from k is 3.

Step 2 Get forecasting disturbances for M_2 measurement points, $\widetilde{\varepsilon}_{\mathbf{k+1}}$, by process error $\mathbf{e}_k$ and the MIMO time–effect controller.

Step 3 Set $\widehat{F}_{2,k+1}$ to $\widehat{F}_2$ from Eq. (12).

Step 4 Modify the MIMO time–effect forecasting process disturbances at run $k+1$ using Eq. (8), where $\widetilde{\varepsilon}_{k+1}$ is obtained by step 2 and $\widehat{F}_{2,k+1}$ is obtained by step 3.

Step 5: Determine the recipe $\mathbf{X}_{k+1}$ using Eqs. (10) or (11). Then, obtain process error $\mathbf{e}_{k+1}$ at run $k+1$.

Step 6: Let $k=k+1$ and repeat steps 2–5 to produce the follow-up recipes.

4 Stability analysis

EWMA is chosen as time–effect controller to analyze stability region of STC. For the other time–effect controllers, same procedures can be applied. We first derive transfer function from the block diagram for MIMO plants and then discuss the stability region under different model mismatch, discount factor, and two-dimensional propagation parameter. Finally, intrinsic properties of EWMA and STC are compared.

4.1 Transfer function

The closed-loop transfer function of STC, recipe generator, and plant can be derived from Fig. 5 directly by Matlab solution [31] with 36 nodes assigned (number 1–36 in Fig. 5). However, while implementing [31] into Fig. 5, Matlab shows "maximum variable size allowed by the program is exceeded". So, this study redraws a MIMO signal flow graph by reducing 36 nodes to 3 nodes. In Fig. 7, node A represents nodes 1–12 in Fig. 5, node B represents nodes 13–24 in Fig. 5, and node C represents nodes 25–36 in Fig. 5. Furthermore, H_1 is the path gain from T to node 1–12 in Fig. 5. H_2 involves MIMO plant and controller. H_3 and H_4 are unity gains and negative feedbacks (1 and −1 s) of producing

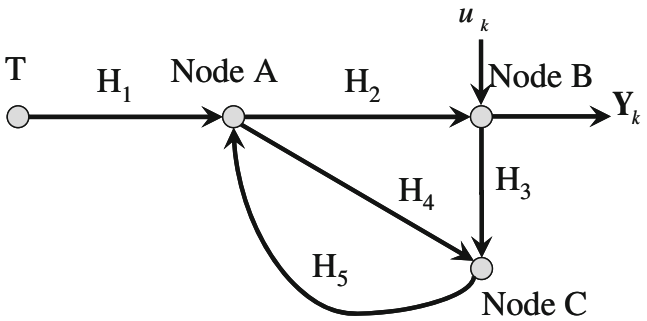

Fig. 7 The MIMO signal–flow graph of Fig. 5

process error. H_5 is controller of STC. Then, the transfer function from disturbance to output, G_{dy}, can be obtained:

$$G_{\mathrm{dy}} = I - H_2/(I - H_5H_4 - H_5H_3H_2)H_5H_3 \tag{13}$$

where

$$H_1 = \begin{bmatrix} G_1 & 0 & \cdots & \cdots & 0 \\ G_2 & 0 & & & 0 \\ \vdots & & \ddots & & \vdots \\ \vdots & & & \ddots & \vdots \\ G_{12} & 0 & \cdots & \cdots & 0 \end{bmatrix},$$

$H_2 = \beta\left(\widehat{\beta}^{\mathrm{T}}\widehat{\beta}\right)^{-1}\widehat{\beta}^{\mathrm{T}}$ when $M_2 \geq N_2$ and $H_2 = \beta\widehat{\beta}^{\mathrm{T}}\left(\widehat{\beta}\widehat{\beta}^{\mathrm{T}}\right)^{-1}$ when $\mathrm{M}_2 \leq \mathrm{N}_2$,

$$H_3 = \begin{bmatrix} G_{25,13} & 0 & \cdots & \cdots & 0 \\ 0 & G_{26,14} & & & 0 \\ \vdots & & \ddots & & \vdots \\ \vdots & & & \ddots & \vdots \\ 0 & 0 & \cdots & \cdots & G_{36,24} \end{bmatrix},$$

$$H_4 = \begin{bmatrix} G_{25,1} & 0 & \cdots & \cdots & 0 \\ 0 & G_{26,2} & & & 0 \\ \vdots & & \ddots & & \vdots \\ \vdots & & & \ddots & \vdots \\ 0 & 0 & \cdots & \cdots & G_{36,12} \end{bmatrix} \text{ and}$$

$$H_5 = \begin{bmatrix} G_{1,25} & G_{1,26} & \cdots & \cdots & G_{1,36} \\ G_{2,25} & G_{2,26} & & & G_{2,36} \\ \vdots & & \ddots & & \vdots \\ \vdots & & & \ddots & \vdots \\ G_{12,25} & G_{12,26} & \cdots & \cdots & G_{12,36} \end{bmatrix}.$$

In Eq. (13), G_i is the path gain of the ith forward path; $G_{i,j}$ is the path gain from node j to node i in Fig. 5; β and $\widehat{\beta}$ are

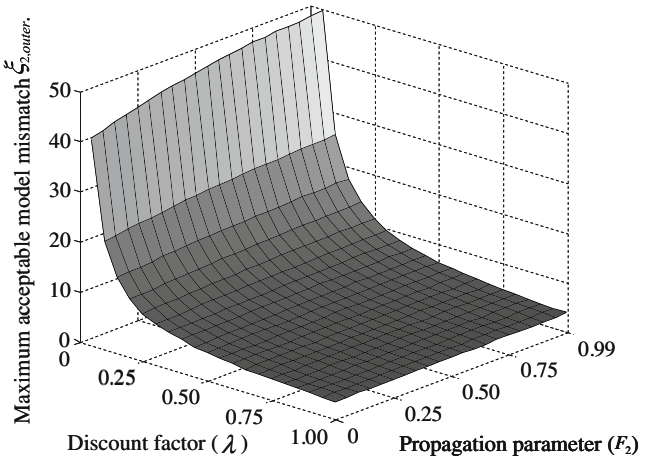

(a) $\mathrm{M}_2 > \mathrm{N}_2$

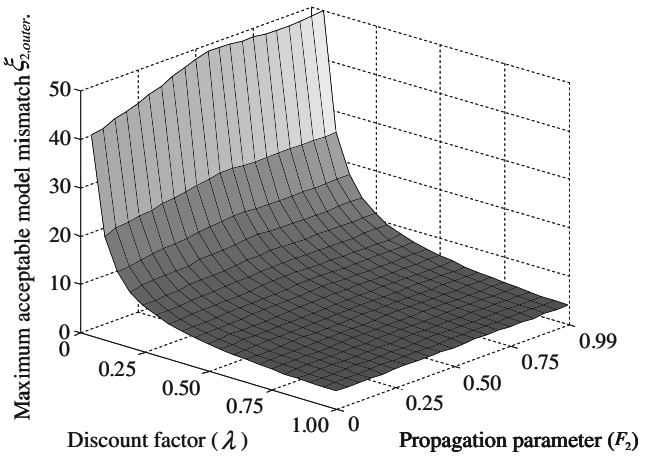

(b) $\mathrm{M}_2 < \mathrm{N}_2$

Fig. 8 3D plot of stability region of STC in the *outer circle*, when $\xi_{\mathrm{outer}} = 1.5 \times \xi_{\mathrm{inner}}$. **a** Stable region of STC in the *outer circle*, when $\xi_{\mathrm{outer}} = 1.5 \times \xi_{\mathrm{inner}}$ and $M_2 > N_2$. **b** Stable region of STC in the outer circle, when $\xi_{\mathrm{outer}} = 1.5 \times \xi_{\mathrm{inner}}$ and $M_2 < N_2$. **c** Stable region of STC in the outer circle, when $\lambda = 0.3$ and $M_2 > N_2$. **d** Stable region of STC in the outer circle, when $\lambda = 0.3$ and $M_2 < N_2$

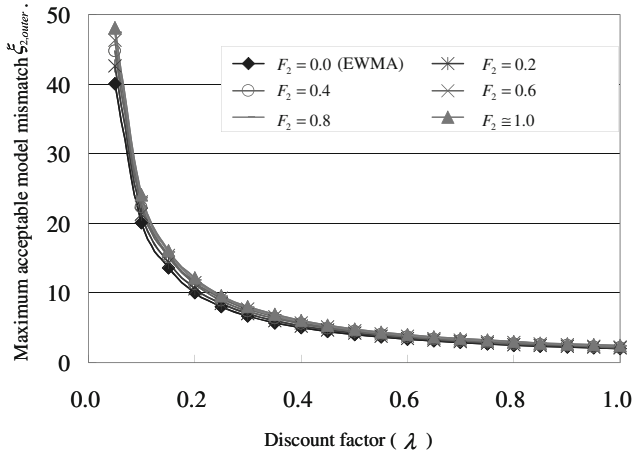

(a) Stable region of STC in the outer circle, when $\xi_{outer} = 1.5 \times \xi_{inner}$ and $M_2 > N_2$.

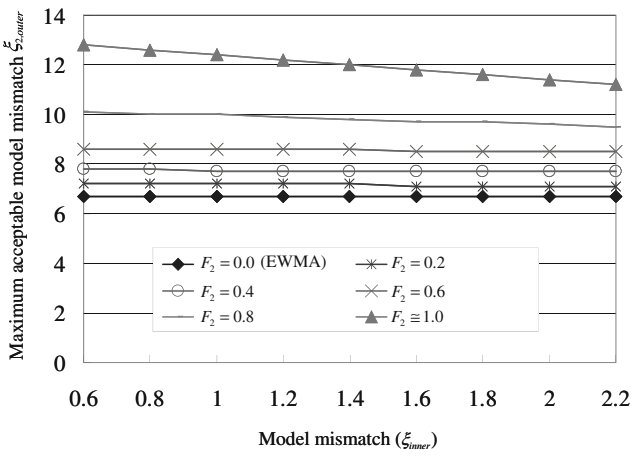

(c) Stable region of STC in the outer circle, when $\lambda = 0.3$ and $M_2 > N_2$.

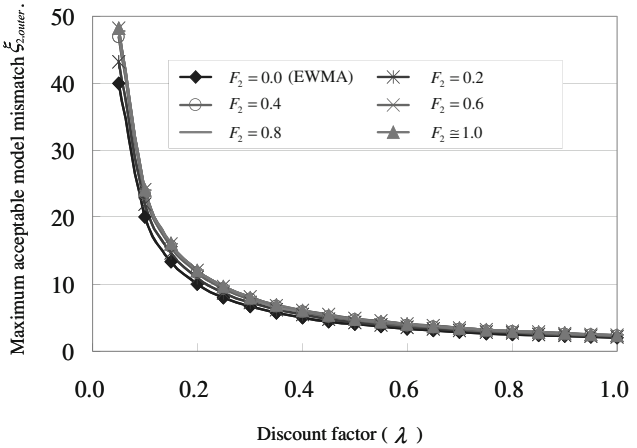

(b) Stable region of STC in the outer circle, when $\xi_{outer} = 1.5 \times \xi_{inner}$ and $M_2 < N_2$.

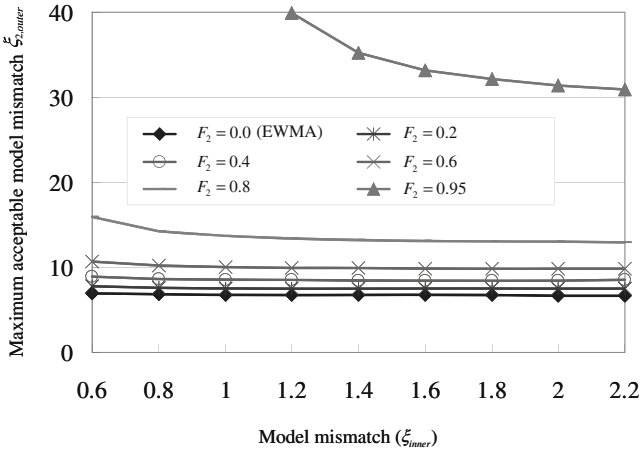

(d) Stable region of STC in the outer circle, when $\lambda = 0.3$ and $M_2 < N_2$.

Fig. 9 Stability region of STC (EWMA with 2D-PPC) for the given conditions in Section 4.2. **a** One set of anthropogenic disturbance. **b** Anthropogenic disturbances of 27 successive runs, where 12 measurement positions are conducted for each wafer

Table 2 Controller structure comparison of time–effect controller (EWMA) and STC (EWMA with 2D-PCC)

Concept	Controllers in this study	Controller parameters		Pole number	Zero number	Controller type	Allowable stable region for all controller parameters
		λ	F_2				
Time–effect controller	MIMO EWMA	If $\mathbf{\Lambda}=\lambda\mathbf{I}$, $0 \leqq \lambda \leqq 1$	NA	$\min(M_2, N_2)$	$\min(M_2, N_2)$	MIMO EWMA is a MIMO integral controller.	If $\beta = \widehat{\xi\beta}$ and $\mathbf{\Lambda}=\lambda\mathbf{I}$, $\xi\lambda \leq 2$.
STC	MIMO EWMA with 2D-PPC	If $\mathbf{\Lambda}=\lambda\mathbf{I}$, $0 \leqq \lambda \leqq 1$	$F_2=0$	The space-effect controller is disable and the control loop is equal to the time-effect controller			
		If $\mathbf{\Lambda}=\lambda\mathbf{I}$, $0 \leqq \lambda \leqq 1$	$0<F_2<1$	$\min(M_2, N_2)$	$\min(M_2, N_2)$	STC is a MIMO integral controller and has $\sum_{1}^{\min(M_2,N_2)} M_1$ poles and zeros (M_1 varies by different controllers and is 1 for EWMA)	Stable region increases with the growth of F_2
		If $\mathbf{\Lambda}=\lambda\mathbf{I}$, $0 \leqq \lambda \leqq 1$	$F_2 \to 1$	$\min(M_2, N_2)$	$\min(M_2, N_2)$	When F_2 approaches to 1, the 2D-PPC is equal to a M_2 moving average filter among M_2 disturbances of EWMA	

defined in Sections 3.1 and 3.4. The values of notations in Eq. (13) are listed at no. 13–19 of Table 1.

4.2 Stability region

The stability region of Fig. 5 can be obtained by checking the pole locations of the transfer function, Eq. (13). We examine the stability region of STC in terms of model mismatch ($\beta = \xi\widetilde{\beta}$) with different values of λ and F_2. If all of the poles are within the unit circle, the point (λ, F_2, ξ) is a stable point.

To simplify analysis, β_{outer} and β_{inner} denote the system gains of the measurement points at the outer circle (positions 1–6) and at the inner circle (positions 7–12) in Fig. 2. Then, β becomes,

$$\beta = \begin{bmatrix} \beta_{\mathbf{outer}} \\ \beta_{\mathbf{inner}} \end{bmatrix}. \tag{14}$$

In Eq. (14), the size of β_{outer} and β_{inner} are both $(M_2/2) \times N_2$. Next, this study assumes that model mismatch of the outer and inner circle, ξ_{outer} and ξ_{inner}, are

$$\beta_{\text{outer}} = \xi_{\text{outer}}\widehat{\beta}_{\text{outer}} \tag{15}$$

$$\beta_{\text{inner}} = \xi_{\text{inner}}\widehat{\beta}_{\text{inner}} \tag{16}$$

Fig. 10 Anthropogenic disturbance in the simulation

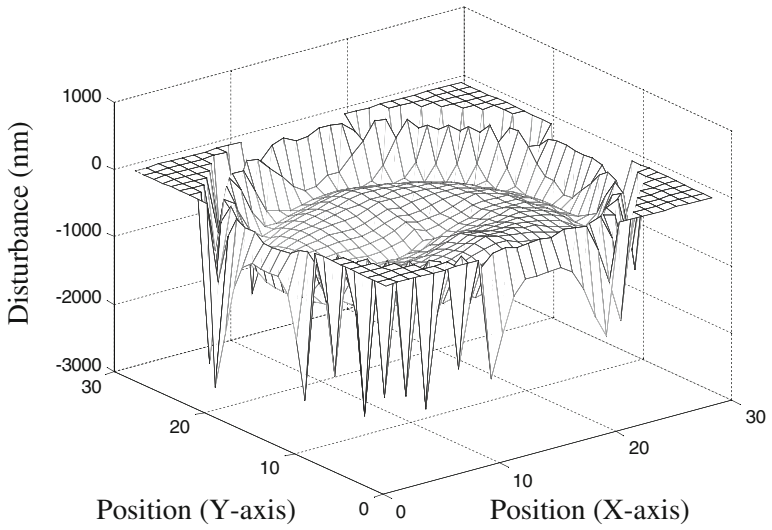

(a) One set of anthropogenic disturbance.

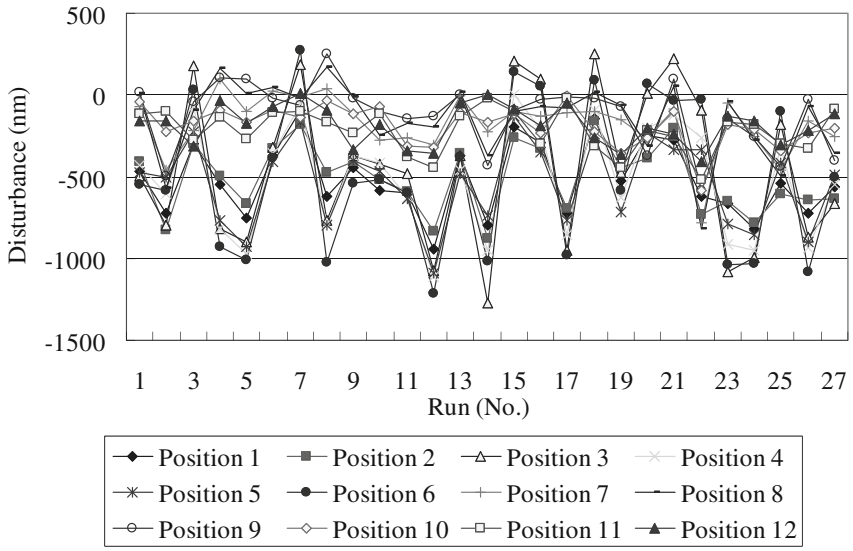

(b) Anthropogenic disturbances of 27 successive runs, where 12 measurement positions are conducted for each wafer.

Table 3 The settings of the MIMO plant and model for the simulations

Settings								
The first MIMO plant ($M_2>N_2$)	$\alpha=[\alpha_1 \cdots \alpha_6 \ \alpha_7 \cdots \alpha_{12}]^{\mathrm{T}}=[6700.26 \cdots 6700.26 \ 4304.63 \cdots 4304.63]^{\mathrm{T}}$							
	β_{m_2,n_2}	n_2=1	n_2=2	β_{m_2,n_2}	n_2=1	n_2=2	β_{m_2,n_2}	n_2=1	n_2=2
	m_2=1	−1,356.6	1,182.2	m_2=5	−1,356.6	1,182.2	m_2=9	85.54	−1,458.8
	m_2=2	−1,356.6	1,182.2	m_2=6	−1,356.6	1,182.2	m_2=10	85.54	−1,458.8
	m_2=3	−1,356.6	1,182.2	m_2=7	85.54	−1,458.8	m_2=11	85.54	−1,458.8
	m_2=4	−1,356.6	1,182.2	m_2=8	85.54	−1,458.8	m_2=12	85.54	−1,458.8
The second MIMO plan ($M_2<N_2$)	$\alpha=[\alpha_1 \cdots \alpha_6 \ \alpha_7 \cdots \alpha_{12}]^{\mathrm{T}}=[6,700.26 \cdots 6,700.26 \ 4,304.63 \cdots 4,304.63]^{\mathrm{T}}$							
	β_{m_2,n_2}	n_2=1	n_2=2	n_2=3	n_2=4	n_2=5	n_2=6	n_2=7	n_2=8
	m_2=1	−111.55	106.64	−109.33	105.20	−110.98	102.12	−107.77	99.75
	m_2=2	−109.51	104.93	−111.77	103.38	−103.23	105.14	−104.72	103.59
	m_2=3	−108.29	102.98	−107.17	102.72	−108.16	98.90	−106.50	106.42
	m_2=4	−112.08	99.27	−110.12	107.35	−105.29	107.28	−107.90	107.89
	m_2=5	−103.48	99.30	−112.42	104.43	−110.55	106.06	−106.60	105.24
	m_2=6	−103.49	99.97	−111.15	106.55	−108.94	107.88	−109.81	100.23
	m_2=7	−109.17	106.72	−106.11	101.37	−107.61	105.47	−112.74	101.19
	m_2=8	−104.01	103.39	−110.39	107.76	−108.33	102.90	−105.12	101.90
	m_2=9	−106.53	102.53	−111.30	99.87	−111.33	100.97	−108.55	106.24
	m_2=10	−105.45	107.66	−105.27	106.07	−105.21	100.04	−109.91	100.62
	m_2=11	−104.18	107.12	−112.36	102.43	−107.11	106.80	−112.55	103.18
	m_2=12	−106.70	103.79	−111.33	101.47	−106.27	100.66	−110.05	108.12
	β_{m_2,n_2}	n_2=9	n_2=10	n_2=11	n_2=12	n_2=13	n_2=14	n_2=15	n_2=16
	m_2=1	−104.29	103.44	−108.49	104.38	16.31	−118.08	10.62	−111.87
	m_2=2	−111.41	104.92	−112.40	98.80	8.33	−118.34	10.84	−114.80
	m_2=3	−110.03	101.38	−110.93	100.77	10.39	−119.68	14.70	−119.29
	m_2=4	−110.87	100.49	−104.24	105.46	15.99	−116.28	7.85	−115.25
	m_2=5	−107.31	102.72	−107.95	100.69	15.96	−118.26	17.05	−115.25
	m_2=6	−103.51	102.19	−107.42	104.31	9.39	−113.18	8.35	−120.98
	m_2=7	−109.00	107.36	−110.03	104.42	7.16	−116.02	12.36	−120.16
	m_2=8	−108.29	99.09	−110.20	102.20	13.59	−121.12	12.54	−111.86
	m_2=9	−111.65	107.16	−104.63	105.13	12.90	−120.48	13.99	−117.09
	m_2=10	−109.96	107.54	−105.10	101.29	7.83	−119.38	16.58	−120.76
	m_2=11	−103.88	106.69	−111.60	101.51	9.19	−121.00	15.23	−118.80
	m_2=12	−103.09	100.63	−104.63	103.13	15.47	−118.17	15.85	−119.31
	β_{m_2,n_2}	n_2=17	n_2=18	n_2=19	n_2=20	n_2=21	n_2=22	n_2=23	n_2=24
	m_2=1	9.85	−121.22	13.57	−121.38	12.58	−114.67	8.47	−115.36
	m_2=2	8.26	−117.69	9.88	−118.88	9.48	−119.41	8.18	−117.01
	m_2=3	12.73	−116.30	7.63	−114.26	8.92	−115.75	14.43	−121.52
	m_2=4	11.23	−119.47	16.83	−116.52	16.83	−120.77	7.32	−117.71
	m_2=5	10.59	−112.10	16.94	−118.52	13.02	−115.21	12.47	−111.92
	m_2=6	7.98	−120.33	14.19	−114.37	12.66	−119.06	10.67	−117.51
	m_2=7	8.89	−114.38	14.34	−119.14	8.79	−120.32	13.03	−111.57
	m_2=8	15.42	−116.01	11.00	−120.22	11.41	−121.17	8.33	−117.14
	m_2=9	7.99	−116.84	13.25	−116.71	16.22	−119.72	16.74	−116.60
	m_2=10	13.94	−117.01	16.07	−121.39	7.97	−119.60	11.29	−111.97
	m_2=11	11.49	−118.76	12.53	−116.31	12.58	−119.30	8.89	−119.20
	m_2=12	16.44	−117.72	8.85	−117.21	10.22	−119.99	8.99	−112.18

Table 4 Simulation results of the first MIMO plant ($M_2>N_2$) for Example 1

SSE (nm) of controlled outputs		MIMO EWMA 3.64E+07	MIMO EWMA with 2D-PPC 3.59E+07	Improvement (%) 1.27	MIMO PCC 3.64E+07	MIMO PCC with 2D-PCC 3.31E+07	Improvement (%) 9.05	MIMO dEWMA 3.64E+07	MIMO dEWMA with 2D-PPC 3.59E+07	Improvement (%) 1.34
Controller parameters	F_2	NA	0.18	NA	NA	NA	NA	NA	NA	NA
	$F_{2,s}$	NA	NA	NA	NA	0.99	NA	NA	0.23	NA
	$F_{2,d}$	NA	NA	NA	NA	0.45	NA	NA	0.00	NA
	λ	0.48	0.51	NA	NA	NA	NA	NA	NA	NA
	λ_1	NA	NA	NA	0.00	0.00	NA	0.48	0.5	NA
	λ_2	NA	NA	NA	0.48	0.52	NA	0.00	0.01	NA

Thus, there are four parameters, ξ_{outer}, ξ_{inner}, λ, and F_2, in Eq. (13); when two of them are given, stability region among the three other parameters can be presented in a 3-D plot. For example, when $\xi_{\text{outer}}=1.5\times\xi_{\text{inner}}$ and $\lambda=0.3$, the maximum acceptable model mismatches of STC in the outer, $\widehat{\xi}_{2,\text{outer}}$, shown in shaded curved surface, for different F_2 and λ are presented in Fig. 8a–b, where the stability region is under the shaded curved surface. The cross-sections perpendicular to the $F_2-\lambda$ plane and parallel to the $\widehat{\xi}_{2,\text{outer}}-\lambda$ plane in terms of various F_2 are shown in Fig. 9a–b. In Fig. 9a–b, $\widehat{\xi}_{2,\text{outer}}$ decreases with the growth of λ but increases with the growth of F_2. In Fig. 9c–d, $\widehat{\xi}_{2,\text{outer}}$ decreases with the growth of ξ_{inner} but still increases with the growth of F_2. In sum, it shows that STC increases the stability region at the outer circle by the growth of F_2 as compared to EWMA, which is the region under the curve when $F_2=0$. Note that the conclusion is also applied to the stability regions at the inner circle by the same token.

The intrinsic properties of STC and EWMA are given in Table 2 including the number of poles and zeros of STC examined from Eq. (13), EWMA and the controller type. The MIMO EWMA is a MIMO integral controller, while STC varies with the 2D propagation parameter F_2. When F_2 is zero, the space–effect controller is disable and the control loop is equal to MIMO EWMA. When F_2 is not zero, the number of pole or zero of STC becomes $\sum_{1}^{\min(M_2,N_2)} M_1$ and one of the zero positions is 1. Thus, STC preserves the property of EWMA in step disturbance rejection. As F_2 of STC approaches to 1, the 2D-PPC is equal to a M_2 moving average filter among M_2 disturbances of EWMA.

5 Simulation results

To do the simulation, this study makes 27 sets of anthropogenic disturbance from fabrication data to examine output performance of the six candidate controllers. Figure 10a is a set of anthropogenic disturbance and Fig. 10b is the anthropogenic disturbances of 27 successive runs, where 12 measurement positions are conducted for each wafer. This paper conducts two simulations for two types of MIMO plants ($M_2>N_2$ and $M_2<N_2$) to compare output performance of the candidate controllers. In the first example, with different model mismatch at the measurement positions in the inner and outer circles,

Table 5 Simulation results of the second MIMO plant ($M_2<N_2$) for Example 1

SSE (nm) of controlled outputs		MIMO EWMA 9.13E+07	MIMO EWMA with 2D-PPC 6.75E+07	Improvement (%) 26.06	MIMO PCC 9.13E+07	MIMO PCC with 2D-PCC 6.16E+07	Improvement (%) 32.52	MIMO dEWMA 9.13E+07	MIMO dEWMA with 2D-PPC 6.49E+07	Improvement (%) 28.89
Controller parameters	F_2	NA	0.19	NA	NA	NA	NA	NA	NA	NA
	$F_{2,s}$	NA	NA	NA	NA	0.76	NA	NA	0.63	NA
	$F_{2,d}$	NA	NA	NA	NA	0.65	NA	NA	0	NA
	λ	0.45	0.41	NA	NA	NA	NA	NA	NA	NA
	λ_1	NA	NA	NA	0.45	0	NA	0.45	0.37	NA
	λ_2	NA	NA	NA	0	0.34	NA	0	0.01	NA

Table 6 Simulation results of the first MIMO plant ($M_2>N_2$) for example 2

SSE (nm) of controlled outputs		MIMO EWMA	MIMO EWMA with 2D-PPC	Improvement (%)	MIMO PCC	MIMO PCC with 2D-PCC	Improvement (%)	MIMO dEWMA	MIMO dEWMA with 2D-PPC	Improvement (%)
		3.05E+07	3.01E+07	1.53	3.05E+07	2.81E+07	7.81	3.05E+07	3.01E+07	1.53
Controller parameters	F_2	NA	0.34	NA	NA	NA	NA	NA	NA	NA
	$F_{2,s}$	NA	NA	NA	NA	0.03	NA	NA	0.34	NA
	$F_{2,d}$	NA	NA	NA	NA	0.99	NA	NA	0.00	NA
	λ	0.27	0.31	NA	NA	NA	NA	NA	NA	NA
	λ_1	NA	NA	NA	0.00	0.00	NA	0.27	0.31	NA
	λ_2	NA	NA	NA	0.27	0.35	NA	0.00	0.00	NA

one investigates the effect of the model mismatch on the performance. In the second example, an additional impulse disturbance at run 10 of measurement position 6 is added to investigate the effect of disturbance on the performance. The process target T was 4,500 nm and the settings of two MIMO plants are listed at Table 3.

This section compares the performances of MIMO EWMA, MIMO dEWMA, and MIMO PCC with and without 2D-PPC for the two types of MIMO plants. In MIMO dEWMA and MIMO PCC with 2D-PPC, $\Lambda_1=\lambda_1 I$ and $\Lambda_2=\lambda_2 I$ are discount factors of the shift and drift terms, respectively and $F_{2,s}$ and $F_{2,d}$ are the two 2D propagation parameters of the shift terms and the drift terms of a wafer independently. Finally, this study employs SSE to evaluate the output performance.

5.1 Performance comparison with different model mismatches within a wafer

The first simulation compares output performance of twelve candidate controllers with $\xi_{\text{inner}}=1.2$ and $\xi_{\text{outer}}=1.5$. The controller parameters can be obtained from anthropogenic disturbance by Eq. (12). Then, the optimal control parameters are applied to the same simulated data. Controller parameters with output performance for the two MIMO plants are listed in Tables 4 and 5 in which simulation results are divided into three groups: (1) EWMA and EWMA with 2D-PPC, (2) dEWMA and dEWMA with 2D-PPC, and (3) PCC and PCC with 2D-PPC. It is observed that the output performances of STC for three groups are all better than those of traditional MIMO time–effect controllers.

5.2 Performance comparison with an additional impulse disturbance within a wafer

To show the advantage of space–effect controller, this example adds an additional impulse disturbance 1,000 at run 10 of measurement position 6. The simulation assumes that model mismatches of the all measurement positions are 1.2. The optimal controller parameters is also obtained from Eq. (12). Controller parameters with

Table 7 Simulation results of the second MIMO plant ($M_2<N_2$) for example 2

SSE (nm) of controlled outputs		MIMO EWMA 4.53E+07	MIMO EWMA with 2D-PPC 4.01E+07	Improvement (%) 11.46	MIMO PCC 4.53E+07	MIMO PCC with 2D-PCC 3.73E+07	Improvement (%) 17.50	MIMO dEWMA 4.53E+07	MIMO dEWMA with 2D-PPC 4.01E+07	Improvement (%) 11.46
Controller parameters	F_2	NA	0.66	NA	NA	NA	NA	NA	NA	NA
	$F_{2,s}$	NA	NA	NA	NA	0.83	NA	NA	0.66	NA
	$F_{2,d}$	NA	NA	NA	NA	0.93	NA	NA	0	NA
	λ	0.45	0.35	NA	NA	NA	NA	NA	NA	NA
	λ_1	NA	NA	NA	0.45	0.00	NA	0.45	0.35	NA
	λ_2	NA	NA	NA	0.0	0.39	NA	0.00	0.00	NA

output performance for the two MIMO plants are listed in Tables 6 and 7. One observes that, when the wafer has an additional impulse disturbance, the STC improves the output performance over the MIMO time–effect controller in all three groups for the given plants.

6 Conclusions

In this paper, the 2D-PPC is developed to realize space–effect controller, and then it is interlaced with the MIMO time–effect controller to establish the framework of the STC. From implementation view point, since STC does not change the original code of time–effect controller, it can be easily implemented in the current process control loop by only adding an additional space–effect controller to obtain new modified intercept for the subsequent use in the MIMO time–effect controller. The advantages we gain are that STC not only preserves the property of the MIMO time–effect controller but also increases the stable region and performs better as compared to time–effect controller.

Appendix A

To overcome the end effect of the transition function [22], we modify the propagation-out ratio at the frontier points from $F_2/(2-F_2)$ [22] to Γ. Without loss of generality, this study takes the shape of the two-dimensional pheromone basket is shown as Fig. 2 and $\mathbf{R_2}(k,0)$ is the 12×1 matrix of 1s as an example. The transition functions are

$$q_2(k,b_{m_2},i+1)=\begin{cases}\frac{F_2}{3}\left(r_2(k,b_{m_2+6},i)+q_2(k,b_{m_2+6},i)\right), & \text{if } m_2=1,2,\ldots,6\\ \Gamma\left(r_2(k,b_{m_2-6},i)+q_2(k,b_{m_2-6},i)\right)+\frac{F_2}{3}\left(r_2(k,b_{m_2+1},i)+q_2(k,b_{m_2+1},i)\right)\\ +\frac{F_2}{3}\left(r_2(k,b_{m_2-1},i)+q_2(k,b_{m_2-1},i)\right), & \text{if } m_2=8,9,\ldots,11\\ \Gamma\left(r_2(k,b_{m_2-6},i)+q_2(k,b_{m_2-6},i)\right)+\frac{F_2}{3}\left(r_2(k,b_{m_2+1},i)+q_2(k,b_{m_2+1},i)\right)\\ +\frac{F_2}{3}\left(r_2(k,b_{12},i)+q_2(k,b_{12},i)\right), & \text{if } m_2=7\\ \Gamma\left(r_2(k,b_{m_2-6},i)+q_2(k,b_{m_2-6},i)\right)+\frac{F_2}{3}\left(r_2(k,b_7,i)+q_2(k,b_7,i)\right)\\ +\frac{F_2}{3}\left(r_2(k,b_{m_2-1},i)+q_2(k,b_{m_2-1},i)\right), & \text{if } m_2=12\end{cases} \tag{A.1}$$

$$s_2(k,b_{m_2},i+1)=\begin{cases}s_2(k,b_{m_2},i)+(1-\Gamma)\left(r_2(k,b_{m_2},i)+q_2(k,b_{m_2},i)\right), & \text{if} m_2=1,2,...6\\ s_2(k,b_{m_2},i)+(1-F_2)\left(r_2(k,b_{m_2},i)+q_2(k,b_{m_2},i)\right), & \text{if} m_2=7,8,...,12\end{cases} \tag{A.2}$$

Next, Eq. (A.2) can be rewrote as

$$\begin{bmatrix}\mathbf{Q_2}(k,i+1)\\ \mathbf{S_2}(k,i+1)\end{bmatrix}=\begin{bmatrix}\mathbf{T_{11}} & \mathbf{T_{12}}\\ \mathbf{T_{21}} & \mathbf{T_{22}}\end{bmatrix}\begin{bmatrix}\mathbf{Q_2}(k,i)\\ \mathbf{S_2}(k,i)\end{bmatrix}+\begin{bmatrix}\mathbf{U_{11}} & \mathbf{U_{12}}\\ \mathbf{U_{21}} & \mathbf{U_{22}}\end{bmatrix}\begin{bmatrix}\mathbf{R_2}(k,i)\\ \mathbf{R_2}(k,i)\end{bmatrix}, \tag{A.3}$$

where

$$\mathbf{Q_2}(k,i)=\begin{bmatrix}q_2(k,b_1,i)\\ q_2(k,b_2,i)\\ \vdots\\ q_2(k,b_{12},i)\end{bmatrix},\quad \mathbf{S_2}(k,i)=\begin{bmatrix}s_2(k,b_1,i)\\ s_2(k,b_2,i)\\ \vdots\\ s_2(k,b_{12},i)\end{bmatrix},\quad \mathbf{R_2}(k,i)=\begin{bmatrix}r_2(k,b_1,i)\\ r_2(k,b_2,i)\\ \vdots\\ r_2(k,b_{12},i)\end{bmatrix},$$

$$\mathbf{T_{11}} = \begin{bmatrix} 0 & 0 & 0 & 0 & 0 & 0 & \frac{F_2}{3} & 0 & 0 & 0 & 0 & 0 \\ 0 & 0 & 0 & 0 & 0 & 0 & 0 & \frac{F_2}{3} & 0 & 0 & 0 & 0 \\ 0 & 0 & 0 & 0 & 0 & 0 & 0 & 0 & \frac{F_2}{3} & 0 & 0 & 0 \\ 0 & 0 & 0 & 0 & 0 & 0 & 0 & 0 & 0 & \frac{F_2}{3} & 0 & 0 \\ 0 & 0 & 0 & 0 & 0 & 0 & 0 & 0 & 0 & 0 & \frac{F_2}{3} & 0 \\ 0 & 0 & 0 & 0 & 0 & 0 & 0 & 0 & 0 & 0 & 0 & \frac{F_2}{3} \\ \Gamma & 0 & 0 & 0 & 0 & 0 & 0 & \frac{F_2}{3} & 0 & 0 & 0 & \frac{F_2}{3} \\ 0 & \Gamma & 0 & 0 & 0 & 0 & \frac{F_2}{3} & 0 & \frac{F_2}{3} & 0 & 0 & 0 \\ 0 & 0 & \Gamma & 0 & 0 & 0 & 0 & \frac{F_2}{3} & 0 & \frac{F_2}{3} & 0 & 0 \\ 0 & 0 & 0 & \Gamma & 0 & 0 & 0 & 0 & \frac{F_2}{3} & 0 & \frac{F_2}{3} & 0 \\ 0 & 0 & 0 & 0 & \Gamma & 0 & 0 & 0 & 0 & \frac{F_2}{3} & 0 & \frac{F_2}{3} \\ 0 & 0 & 0 & 0 & 0 & \Gamma & \frac{F_2}{3} & 0 & 0 & 0 & \frac{F_2}{3} & 0 \end{bmatrix}, \mathbf{T_{12}} = \mathbf{0_{12\times 12}},$$

$$\mathbf{T_{21}} = \begin{bmatrix} 1-\Gamma & 0 & 0 & 0 & 0 & 0 & 0 & 0 & 0 & 0 & 0 & 0 \\ 0 & 1-\Gamma & 0 & 0 & 0 & 0 & 0 & 0 & 0 & 0 & 0 & 0 \\ 0 & 0 & 1-\Gamma & 0 & 0 & 0 & 0 & 0 & 0 & 0 & 0 & 0 \\ 0 & 0 & 0 & 1-\Gamma & 0 & 0 & 0 & 0 & 0 & 0 & 0 & 0 \\ 0 & 0 & 0 & 0 & 1-\Gamma & 0 & 0 & 0 & 0 & 0 & 0 & 0 \\ 0 & 0 & 0 & 0 & 0 & 1-\Gamma & 0 & 0 & 0 & 0 & 0 & 0 \\ 0 & 0 & 0 & 0 & 0 & 0 & 1-F_2 & 0 & 0 & 0 & 0 & 0 \\ 0 & 0 & 0 & 0 & 0 & 0 & 0 & 1-F_2 & 0 & 0 & & 0 \\ 0 & 0 & 0 & 0 & 0 & 0 & 0 & 0 & 1-F_2 & 0 & 0 & 0 \\ 0 & 0 & 0 & 0 & 0 & 0 & 0 & 0 & 0 & 1-F_2 & 0 & 0 \\ 0 & 0 & 0 & 0 & 0 & 0 & 0 & 0 & 0 & 0 & 1-F_2 & 0 \\ 0 & 0 & 0 & 0 & 0 & 0 & 0 & 0 & 0 & 0 & 0 & 1-F_2 \end{bmatrix},$$

$\mathbf{T_{22}} = \mathbf{I_{12\times 12}}$, $\mathbf{U_{11}} = \mathbf{T_{11}}$, $\mathbf{U_{12}} = \mathbf{0_{12\times 12}}$, $\mathbf{U_{21}} = \mathbf{0_{12\times 12}}$, and $\mathbf{U_{22}} = \mathbf{T_{21}}$.

The final propagation result of $\mathbf{V_{12\times 1}}(k)$ obtained from Eq. (A.8) in the Appendix B must be the 12×1 matrix of ones.

$$\mathbf{V_{12\times 1}}(k) = \begin{bmatrix} v_1(k) \\ v_2(k) \\ v_3(k) \\ v_4(k) \\ v_5(k) \\ v_6(k) \\ v_7(k) \\ v_8(k) \\ v_9(k) \\ v_{10}(k) \\ v_{11}(k) \\ v_{12}(k) \end{bmatrix} = \frac{1}{2F_2 + \Gamma F_2 - 3} \begin{bmatrix} (1-\Gamma)(F_2-3) \\ (1-\Gamma)(F_2-3) \\ (1-\Gamma)(F_2-3) \\ (1-\Gamma)(F_2-3) \\ (1-\Gamma)(F_2-3) \\ (1-\Gamma)(F_2-3) \\ 3(1+\Gamma)(F_2-1) \\ 3(1+\Gamma)(F_2-1) \\ 3(1+\Gamma)(F_2-1) \\ 3(1+\Gamma)(F_2-1) \\ 3(1+\Gamma)(F_2-1) \\ 3(1+\Gamma)(F_2-1) \end{bmatrix} = \begin{bmatrix} 1 \\ 1 \\ 1 \\ 1 \\ 1 \\ 1 \\ 1 \\ 1 \\ 1 \\ 1 \\ 1 \\ 1 \end{bmatrix} \tag{A.4}$$

Solving Eq. (A.4) yields,

$$\Gamma = \frac{F_2}{3 - 2F_2} \tag{A.5}$$

Relatively, when $\mathbf{R_2}(k, 0)$ is the 12×1 matrix of ones, Eq. (A.8) becomes

$$\lim_{z\to1}(z-1)Z\{\mathbf{H_2}(k,i)\} = \lim_{z\to1}(z-1)(z\mathbf{I}-\mathbf{T})^{-1}\mathbf{UI_{24\times1}} = \begin{bmatrix}\mathbf{0_{12\times1}}\\ \mathbf{1_{12\times1}}\end{bmatrix}. \tag{A.6}$$

Equation (A.6) shows that the final propagation result $\mathbf{S_2}(k, \infty)$ is also a 12×1 matrix of ones. Thus, the modified transition functions not only obey the energy balance law but also avoid the end effect.

Appendix B

Because states $\mathbf{Q_2}(k, i)$ and $\mathbf{S_2}(k, i)$ are updated simultaneously, the transition functions can be rewritten in matrix form:

$$\begin{bmatrix}\mathbf{Q_2}(k,i+1)\\ \mathbf{S_2}(k,i+1)\end{bmatrix} = \begin{bmatrix}\mathbf{T_{11}} & \mathbf{T_{12}}\\ \mathbf{T_{21}} & \mathbf{T_{22}}\end{bmatrix}\begin{bmatrix}\mathbf{Q_2}(k,i)\\ \mathbf{S_2}(k,i)\end{bmatrix} + \begin{bmatrix}\mathbf{U_{11}} & \mathbf{U_{12}}\\ \mathbf{U_{21}} & \mathbf{U_{22}}\end{bmatrix}\begin{bmatrix}\mathbf{R_2}(k,i)\\ \mathbf{R_2}(k,i)\end{bmatrix}, \tag{A.7}$$

where

$$\mathbf{Q_2}(k,i) = \begin{bmatrix}q_2(k,b_1,i)\\ q_2(k,b_2,i)\\ \vdots\\ q_2(k,b_{12},i)\end{bmatrix},\quad \mathbf{S_2}(k,i) = \begin{bmatrix}s_2(k,b_1,i)\\ s_2(k,b_2,i)\\ \vdots\\ s_2(k,b_{12},i)\end{bmatrix},\quad \mathbf{R_2}(k,i) = \begin{bmatrix}r_2(k,b_1,i)\\ r_2(k,b_2,i)\\ \vdots\\ r_2(k,b_{12},i)\end{bmatrix},$$

$$\mathbf{T_{11}} = \begin{bmatrix}
0 & 0 & 0 & 0 & 0 & 0 & \frac{F_2}{3} & 0 & 0 & 0 & 0 & 0\\
0 & 0 & 0 & 0 & 0 & 0 & 0 & \frac{F_2}{3} & 0 & 0 & 0 & 0\\
0 & 0 & 0 & 0 & 0 & 0 & 0 & 0 & \frac{F_2}{3} & 0 & 0 & 0\\
0 & 0 & 0 & 0 & 0 & 0 & 0 & 0 & 0 & \frac{F_2}{3} & 0 & 0\\
0 & 0 & 0 & 0 & 0 & 0 & 0 & 0 & 0 & 0 & \frac{F_2}{3} & 0\\
0 & 0 & 0 & 0 & 0 & 0 & 0 & 0 & 0 & 0 & 0 & \frac{F_2}{3}\\
\frac{F_2}{3-2F_2} & 0 & 0 & 0 & 0 & 0 & 0 & \frac{F_2}{3} & 0 & 0 & 0 & \frac{F_2}{3}\\
0 & \frac{F_2}{3-2F_2} & 0 & 0 & 0 & 0 & \frac{F_2}{3} & 0 & \frac{F_2}{3} & 0 & 0 & 0\\
0 & 0 & \frac{F_2}{3-2F_2} & 0 & 0 & 0 & 0 & \frac{F_2}{3} & 0 & \frac{F_2}{3} & 0 & 0\\
0 & 0 & 0 & \frac{F_2}{3-2F_2} & 0 & 0 & 0 & 0 & \frac{F_2}{3} & 0 & \frac{F_2}{3} & 0\\
0 & 0 & 0 & 0 & \frac{F_2}{3-2F_2} & 0 & 0 & 0 & 0 & \frac{F_2}{3} & 0 & \frac{F_2}{3}\\
0 & 0 & 0 & 0 & 0 & \frac{F_2}{3-2F_2} & \frac{F_2}{3} & 0 & 0 & 0 & \frac{F_2}{3} & 0
\end{bmatrix},\ \mathbf{T_{12}} = \mathbf{0_{12\times12}},$$

$$\mathbf{T_{21}} = \begin{bmatrix} \frac{3(1-F_2)}{3-2F_2} & 0 & 0 & 0 & 0 & 0 & 0 & 0 & 0 & 0 & 0 & 0 \\ 0 & \frac{3(1-F_2)}{3-2F_2} & 0 & 0 & 0 & 0 & 0 & 0 & 0 & 0 & 0 & 0 \\ 0 & 0 & \frac{3(1-F_2)}{3-2F_2} & 0 & 0 & 0 & 0 & 0 & 0 & 0 & 0 & 0 \\ 0 & 0 & 0 & \frac{3(1-F_2)}{3-2F_2} & 0 & 0 & 0 & 0 & 0 & 0 & 0 & 0 \\ 0 & 0 & 0 & 0 & \frac{3(1-F_2)}{3-2F_2} & 0 & 0 & 0 & 0 & 0 & 0 & 0 \\ 0 & 0 & 0 & 0 & 0 & \frac{3(1-F_2)}{3-2F_2} & 0 & 0 & 0 & 0 & 0 & 0 \\ 0 & 0 & 0 & 0 & 0 & 0 & 1-F_2 & 0 & 0 & 0 & 0 & 0 \\ 0 & 0 & 0 & 0 & 0 & 0 & 0 & 1-F_2 & 0 & 0 & 0 & 0 \\ 0 & 0 & 0 & 0 & 0 & 0 & 0 & 0 & 1-F_2 & 0 & 0 & 0 \\ 0 & 0 & 0 & 0 & 0 & 0 & 0 & 0 & 0 & 1-F_2 & 0 & 0 \\ 0 & 0 & 0 & 0 & 0 & 0 & 0 & 0 & 0 & 0 & 1-F_2 & 0 \\ 0 & 0 & 0 & 0 & 0 & 0 & 0 & 0 & 0 & 0 & 0 & 1-F_2 \end{bmatrix},$$

$$\mathbf{T_{22}} = \mathbf{I_{12\times 12}},\ \mathbf{U_{11}} = \mathbf{T_{11}},\ \mathbf{U_{12}} = \mathbf{0_{12\times 12}},\ \mathbf{U_{21}} = \mathbf{0_{12\times 12}} \text{ and } \mathbf{U_{22}} = \mathbf{T_{21}}.$$

In Eq. (A.7), $\mathbf{Q_2}(k, \infty)$ and $\mathbf{S_2}(k, \infty)$ can be obtained with the z-transform and the final value theorem

$$\begin{aligned} \mathbf{H_2}(k,\infty) &= \lim_{z\to 1}(z-1)Z\{\mathbf{H_2}(k,i)\} \\ &= \lim_{z\to 1}(z-1)(z\mathbf{I}-\mathbf{T})^{-1}\mathbf{U}\begin{bmatrix}\mathbf{R_2}(k,i)\\ \mathbf{R_2}(k,i)\end{bmatrix} = \begin{bmatrix}\mathbf{0_{12\times 1}}\\ \mathbf{V}_{12\times 1}(k)\end{bmatrix}. \end{aligned} \tag{A.8}$$

where $\mathbf{H_2}(k,i) = \begin{bmatrix}\mathbf{Q_2}(k,i)\\ \mathbf{S_2}(k,i)\end{bmatrix}$, $\mathbf{T} = \begin{bmatrix}\mathbf{T_{11}} & \mathbf{T_{12}}\\ \mathbf{T_{21}} & \mathbf{T_{22}}\end{bmatrix}$, $\mathbf{U} = \begin{bmatrix}\mathbf{U_{11}} & \mathbf{U_{12}}\\ \mathbf{U_{21}} & \mathbf{U_{22}}\end{bmatrix}$ and $\mathbf{V_{12\times 1}}(k) = [\,v_1(k) \quad \cdots \quad v_{12}(k)\,]^{\mathrm{T}}$. Note $\mathbf{Q_2}$ (k, ∞) in Eq. (A.8) will converge to the matrix of 0 and $\mathbf{S_2}(k, \infty)$ will converge to $\mathbf{V_{12\times 1}}(k)$. In addition, the z-transform of the external input $Z\{\mathbf{R_2}(k, i)\}$ is equal to $\mathbf{R_2}(k, 0)$ since $\mathbf{R}_2(k, i)$ is an impulse at i=0 by definition in Section 2.1. Thus, $\mathbf{V_{12\times 1}}(k)$ is a function of F_2 and $\mathbf{R_2}(k, 0)$ for a specific M_2. The final propagation results can be obtained analytically using Eq. (A.8).

References

1. Sachs E, Hu A, Ingolfsson A (1995) Run by run control: combining SPC and feedback control. IEEE Trans Semi Manuf 8:26–43
2. Ingolfsson A, Sachs E (1993) Stability and sensitivity of an EWMA controller. J Qual Technol 25(4):271–287
3. Smith T, Boning D (1997) A self-tuning EWMA controller utilizing artificial neural network function approximation techniques. IEEE Trans Comput Packag Manuf Technol C 20:121–132
4. Patel NS, Jenkins ST (2000) Adaptive optimization of RtR controllers: the EWMA example. IEEE Trans Semicond Manuf 13:97–107
5. Castillo ED (2001) Some properties of EWMA feedback quality adjustment schemes for drifting disturbances. J Qual Technol 33 (2):153–166
6. Hsu CC, Su CT (2004) A neural network-based adaptive algorithm on the single EWMA controller. Int J Adv Manuf Technol 23(7–8):586–593
7. Epprecht EK, Simões BFT, Mendes FCT (2010) A variable sampling interval EWMA chart for attributes. Int J Adv Manuf Technol 49(1–4):281–292
8. Wu CF, Hung CM, Chen JH, Lee AC (2008) Advanced process control of the critical dimension in photolithography. Int J Precis Eng Manuf 9:12–18
9. Bulter SW, Stefani JA (1994) Supervisory RtR control of polysilicon gate etch using in situ ellipsometry. IEEE Trans Semi Manuf 7:193–201
10. Castillo ED (1999) Long run and transient analysis of a double EWMA feedback controller. IIE Trans 31(12):1157–1169
11. Chen A, Guo RS (2001) Age-based double EWMA controller and its application to CMP processes. IEEE Trans Semi Manuf 14 (1):11–19
12. Su CT, Hsu CC (2004) A time-varying weights tuning method of the double EWMA controller. Omega 32:473–480
13. Tseng ST, Hsu NJ (2005) Sample-size determination for achieving asymptotic stability of a double EWMA control scheme. IEEE Trans Semicond Manuf 18:104–111
14. Tseng ST, Song W, Chang YC (2005) An initial intercept iteratively adjusted (IIIA) controller: an enhanced double EWMA feedback control scheme. IEEE Trans Semicond Manuf 18(3):448–457
15. Lee AC, Pan YR, Hsieh MT (2011) Output disturbance observer structure applied to run-to-run control for semiconductor manufacturing. IEEE Trans Semicond Manuf 24:27–43
16. Wang XA, Mahajan RL (1996) Artificial neural network model-based RtR process controller. IEEE Trans CPMT—Part C 19 (1):19–26
17. Wang GJ, Yu CH (2006) Developing a neural network-based RtR process controller for chemical-mechanical planarization. Int J Adv Manuf Technol 28(9–10):899–908
18. Wang GJ, Lin BS, Chang KJ (2007) In-situ neural network process controller for copper chemical mechanical polishing. Int J Adv Manuf Technol 32(1–2):42–54
19. Wang J, He QP, Qin SJ, Bode CA, Purdy MA (2005) Recursive least square estimation for RtR control with metrology delay and its application to STI etch process. IEEE Trans Semicond Manuf 18:309–319
20. Chen JH, Kuo TW, Chen TC (2008) Advanced process control of metal sputter deposition using a time series analysis. Int J Adv Manuf Technol 36(5–6):501–509
21. Chen JH, Kuo TW, Lee AC (2007) Run-by-run process control of metal sputter deposition: combining time series and extended Kalman filter. IEEE Trans Semicond Manuf 20:278–285

22. Lee DS, Lee AC (2009) Pheromone propagation controller: the linkage of swarm intelligence and advanced process control. IEEE Trans Semicond Manuf 22(3):357–372
23. Stefani JA, Poarch S, Saxena S, Mozumder P (1996) Advanced process control of a CVD tungsten reactor. IEEE Trans Semicond Manuf 9:366–383
24. Yang L, Sheu SH (2006) Integrating multivariate engineering process control and multivariate statistical process control. Int J Adv Manuf Technol 29(1–2):129–136
25. Tseng ST, Chou RJ, Lee SP (2002) A study on a multivariate EWMA controller. IIE Trans 34:541–549
26. Good RP, Qin SJ (2006) On the stability of MIMO EWMA RtR controllers with metrology delay. IEEE Trans Semicond Manuf 19 (1):78–86
27. Tseng ST, Tsung F, Wu CD (2008) A variable multivariate EWMA controller for run-by-run process adjustment. J Chinese Stat Assoc 46:81–105
28. Castillo ED, Rajagopal R (2002) A multivariate double EWMA process adjustment scheme for drifting processes. IIE Trans 34:1055–1068
29. Brueckner S (2000) Return from the ant: synthetic ecosystems for manufacturing control, Ph.D. dissertation, Humboldt University of Berlin
30. Nagy B (2003) Shortest paths in triangular grids with neighbourhood sequences. J Comput Inf Technol 11:111–122
31. Teixeira MCM, Marchesi HF, Assuncao E (2001) Signal-flow graphs: direct method of reduction and MATLAB implementation. IEEE Trans Educat 44(2):185–190